


ORIGINAL RESEARCH ARTICLE

Voltage-dependent activation of Rac1 by Na_v1.5 channels promotes cell migration

Ming Yang¹ | Andrew D. James^{1,2} | Rakesh Suman³ | Richard Kasproicz³ |
Michaela Nelson^{1,2} | Peter J. O'Toole⁴ | William J. Brackenbury^{1,2} ¹Department of Biology, University of York, York, UK²York Biomedical Research Institute, University of York, York, UK³Phase Focus Ltd, Electric Works, Sheffield Digital Campus, Sheffield, UK⁴Bioscience Technology Facility, Department of Biology, University of York, York, UK**Correspondence**

Dr. William J. Brackenbury, Department of Biology and York Biomedical Research Institute, University of York, Heslington, York YO10 5DD, UK.

Email: william.brackenbury@york.ac.uk

Funding information

Medical Research Council, Grant/Award Number: G1000508; Cancer Research UK, Grant/Award Number: A25922; Radhika V Sreedhar Scholarship

Abstract

Ion channels can regulate the plasma membrane potential (V_m) and cell migration as a result of altered ion flux. However, the mechanism by which V_m regulates motility remains unclear. Here, we show that the Na_v1.5 sodium channel carries persistent inward Na⁺ current which depolarizes the resting V_m at the timescale of minutes. This Na_v1.5-dependent V_m depolarization increases Rac1 colocalization with phosphatidylserine, to which it is anchored at the leading edge of migrating cells, promoting Rac1 activation. A genetically encoded FRET biosensor of Rac1 activation shows that depolarization-induced Rac1 activation results in acquisition of a motile phenotype. By identifying Na_v1.5-mediated V_m depolarization as a regulator of Rac1 activation, we link ionic and electrical signaling at the plasma membrane to small GTPase-dependent cytoskeletal reorganization and cellular migration. We uncover a novel and unexpected mechanism for Rac1 activation, which fine tunes cell migration in response to ionic and/or electric field changes in the local microenvironment.

KEYWORDSbreast cancer, membrane potential, migration, Na_v1.5, Rac1

1 | INTRODUCTION

Cellular morphological changes and migration play key roles in normal physiological processes, including during embryonic development and tissue repair. On the other hand, dysfunctional migration occurs in many disease processes, including cancer metastasis (Bravo-Cordero, Hodgson, & Condeelis, 2012). In particular, mesenchymal migration, which is dependent on polarization and formation of lamellipodial protrusions at the leading edge of cells, enables carcinoma cells to escape from primary tumors into surrounding tissues (Friedl, Locker, Sahai, & Segall, 2012).

Dynamic and adaptable changes in actin polymerization lead to altered stiffness, elongation and branching, which in turn permits acquisition of a mesenchymal phenotype and formation of lamellipodial

protrusions (Krause & Gautreau, 2014). These changes are tightly regulated by a multiplicity of signaling mechanisms which are coordinated by the Rho family of small GTPases (Ridley, 2015). One of the best studied Rho GTPases, Rac1, plays a critical role in regulating lamellipodia formation and migration (Wu et al., 2009). Rac1 cycles between active (GTP-bound) and inactive (GDP-bound) forms, catalyzed by guanine nucleotide exchange factors (GEFs) and GTPase-activating proteins (GAPs), respectively (Marei & Malliri, 2017). Rac1 translocates between cytoplasmic and plasma membrane-bound compartments, with activation predominantly occurring at the plasma membrane (Garcia-Mata, Boulter, & Burridge, 2011). Translocation of Rac1 to the plasma membrane and interaction with phospholipids precede interaction with GEFs and nucleotide exchange/activation (Das et al., 2015). Rac1 is anchored to the inner leaflet of the plasma membrane through its prenylated C-

This is an open access article under the terms of the Creative Commons Attribution License, which permits use, distribution and reproduction in any medium, provided the original work is properly cited.

© 2019 The Authors. *Journal of Cellular Physiology* published by Wiley Periodicals, Inc.

terminus and polybasic motif (van Hennik et al., 2003), which permits interaction with the anionic phospholipids PIP2, PIP3, and phosphatidylserine (Finkielstein, Overduin, & Capelluto, 2006; Heo et al., 2006; Remorino et al., 2017). Localized clustering of PIP2, PIP3, and phosphatidylserine within the plasma membrane thus permits precise spatial and temporal distribution of Rac1 activation (Fair et al., 2011; Kay, Koivusalo, Ma, Wohland, & Grinstein, 2012; Remorino et al., 2017). Rac1 activation gradients within heterogeneous signaling nanodomains in turn regulate cytoskeletal rearrangement, lamellipodia formation and migration through binding to WASP-family verprolin-homologous (WAVE) proteins and activation of the actin-related protein 2/3 (Arp2/3) protein complex (Ehrlich, Hansen, & Nelson, 2002; Machacek et al., 2009; Remorino et al., 2017; Ridley, 2011). However, despite its pivotal role in migration, the cellular mechanisms regulating local Rac1 clustering at the plasma membrane are still incompletely understood.

Another set of proteins that play a key role in regulating cellular migration is ion channels (Schwab, Fabian, Hanley, & Stock, 2012). Changes in ion channel expression and/or activity in cancer cells regulate the plasma membrane potential (V_m) and intracellular signaling cascades as a result of altered ion flux (Brackenbury, 2016; Prevarskaya, Skryma, & Shuba, 2018). Motile cancer cells possess a more depolarized V_m compared with terminally-differentiated noncancer cells (Yang & Brackenbury, 2013). The V_m is functionally instructive in regulating cell cycle progression (Sundelacruz, Levin, & Kaplan, 2009), proliferation (Blackiston, McLaughlin, & Levin, 2009; Zhou et al., 2015), differentiation (Sundelacruz, Levin, & Kaplan, 2008), cytoskeletal reorganization (Chifflet, Correa, Nin, Justet, & Hernandez, 2004; Chifflet, Hernandez, & Grasso, 2005; Chifflet, Hernandez, Grasso, & Cirillo, 2003; Nin, Hernandez, & Chifflet, 2009; Szaszi, Sirokmany, Di Ciano-Oliveira, Rotstein, & Kapus, 2005), tissue morphogenesis, regeneration, and tumorigenesis (Beane, Morokuma, Adams, & Levin, 2011; Beane, Morokuma, Lemire, & Levin, 2013; Cervera, Alcaraz, & Mafe, 2016; Chernet & Levin, 2014; Chernet, Adams, Lobikin, & Levin, 2016; Lobikin, Chernet, Lobo, & Levin, 2012; Lobikin et al., 2015). V_m depolarization controls mitogenic signaling by promoting redistribution of phosphatidylserine and PIP2 in the inner leaflet of the plasma membrane, enhancing nanoclustering and activation of the small GTPase K-Ras (Zhou et al., 2015). However, the mechanisms by which V_m regulates other behaviors, including morphological changes and migration, and the dependency of V_m on altered activity of specific ion channels expressed on nonexcitable cells, remain unclear.

An important class of ion channels in the context of cellular migration is the voltage-gated Na^+ channels (VGSCs). VGSCs contain a pore-forming α subunit ($\text{Na}_v1.1$ – $\text{Na}_v1.9$), together with one or more smaller β subunits ($\beta1$ – $\beta4$; Brackenbury & Isom, 2011; Catterall, Goldin, & Waxman, 2003). The canonical function of VGSCs is to regulate V_m depolarization during the rising phase of action potentials in electrically-excitable cells (Hille, 1992). In addition, VGSCs not only regulate neuronal pathfinding and migration (Brackenbury et al., 2010; Brackenbury, Yuan, O'Malley, Parent, & Isom, 2013; Patel & Brackenbury, 2015), but also regulate the migration of nonexcitable cells (Black & Waxman, 2013). For example, the $\text{Na}_v1.5$ subtype is upregulated in breast cancer cells where it plays a critical role in promoting cellular migration, invasion, and metastasis (Besson et al., 2015; Brackenbury, 2012; Brackenbury, Chioni,

Diss, & Djamgoz, 2007; Fraser et al., 2005; Martin, Ufodiama, Watt, Bland, & Brackenbury, 2015; Nelson, Yang, Dowle, Thomas, & Brackenbury, 2015; Nelson, Yang, Millican-Slater, & Brackenbury, 2015; Roger, Besson, & Le Guennec, 2003). In nonexcitable cancer cells, $\text{Na}_v1.5$ carries a small persistent inward Na^+ current, which would be expected to depolarize the V_m at steady state (Roger et al., 2003; Yang et al., 2012). $\text{Na}_v1.5$ activity promotes motility and invasive behavior through several mechanisms, including MAPK activation (House et al., 2010, 2015), upregulation of CD44 expression (Nelson, Yang, Millican-Slater et al., 2015), and potentiation of Na^+/H^+ exchanger type 1 (NHE1) activity leading to cysteine cathepsin activation (Brisson et al., 2011; Brisson et al., 2013; Gillet et al., 2009). $\text{Na}_v1.5$ also promotes acquisition of an elongate mesenchymal-like phenotype, cortactin phosphorylation and cytoskeletal reorganization (Brisson et al., 2013; Nelson, Yang, Millican-Slater et al., 2015). Taken together, these data point to an important role for both $\text{Na}_v1.5$ and V_m in regulating morphological changes and migration. An important question is, therefore, how migratory behavior is regulated by electrical changes and Na^+ flux at the plasma membrane.

Here, we investigated the role of $\text{Na}_v1.5$ in regulating V_m in nonexcitable breast cancer cells. We report that $\text{Na}_v1.5$ promotes steady state V_m depolarization, which in turn leads to localized activation of Rac1 at the plasma membrane, promoting morphological changes and migration. This study uncovers a novel and unexpected voltage-dependent mechanism for Rac1 activation, which would fine tune cell migration in response to ionic and/or electric field changes in the local microenvironment.

2 | MATERIALS AND METHODS

2.1 | Chemicals

Iberitoxin, NS-1619, tetrodotoxin (TTX) and veratridine were purchased from Alomone Labs. Phenytoin was from Sigma. Ionomycin was from Cayman Chemical. EHT1864 was from Santa Cruz Biotechnology. Drugs were reconstituted as stock solutions according to manufacturer guidelines and diluted directly into culture medium and/or recording solutions at the indicated working concentrations.

2.2 | Cell culture

MDA-MB-231 human breast cancer cells were cultured at 37°C, 5% CO_2 in Dulbecco's modified Eagle's medium (DMEM) supplemented with 5% fetal bovine serum (FBS) and 4 mM L-glutamine. MDA-MB-231 cells are a well-established cell line for examining the functional activity of $\text{Na}_v1.5$ in regulating cell behavior and they demonstrate robust endogenous expression of this channel (Brackenbury et al., 2007; Brisson et al., 2011, 2013; Fraser et al., 2005; Nelson, Millican-Slater, Forrest, & Brackenbury, 2014; Roger et al., 2003; Yang et al., 2012). Cells were confirmed to be mycoplasma-free by the 4',6-diamidino-2-phenylindole (DAPI) staining method (Uphoff, Gignac, & Drexler, 1992). Molecular identity was confirmed by short tandem repeat analysis (Masters et al., 2001).

2.3 | RNA interference

A GFP-expressing MDA-MB-231 cell line lacking functional Na_v1.5 expression was produced previously by transduction of recombinant lentivirus for shRNA targeting Na_v1.5 (MISSION pLKO.1-puro shRNA transduction particles; Sigma) (Nelson, Yang, Millican-Slater et al., 2015). Na_v1.5-shRNA cells and nontargeting shControl cells were maintained in G418 (4 μl/ml, Sigma), blasticidin (2 μl/ml, AppliChem) and puromycin (0.1 μl/ml, Sigma).

2.4 | Whole-cell patch clamp recording

The whole-cell patch clamp technique was used to record membrane current and voltage from cells grown on glass coverslips for 48–72 hr. Voltage- and current-clamp recordings were made using a Multiclamp 700B amplifier (Molecular Devices) at room temperature. Membrane currents and V_m were digitized using a Digidata 1440A interface (Molecular Devices), low-pass filtered at 10 kHz and analyzed using pCLAMP 10.4 software (Molecular Devices). In voltage-clamp mode, signals were sampled at 50 kHz, and the series resistance was compensated by 40–60%. Linear components of leak were subtracted using a P/6 protocol (Armstrong & Bezanilla, 1977). The standard extracellular physiological saline solution (PSS) contained the following components (in mM): 144 NaCl, 5.4 KCl, 1 MgCl₂, 2.5 CaCl₂, 5 HEPES, and 5.6 glucose adjusted to pH 7.2 with NaOH. For the Na⁺-free PSS, NaCl was replaced with 144 mM N-methyl-D-glucamine (NMDG) or choline chloride (ChoCl) adjusted to pH 7.2 with HCl. The standard intracellular (pipette) solution contained (in mM) 5 NaCl, 145 KCl, 2 MgCl₂, 1 CaCl₂, 10 HEPES, and 11 EGTA adjusted to pH 7.4 with KOH. Free Ca²⁺ concentration in the solution was calculated using MaxChelator software (Stanford University). Na⁺ current was activated by depolarizing from –120 mV (250 ms) to voltages in the range –80 to +30 mV in 5 mV increments (50 ms).

2.5 | Membrane potential recording

The steady-state V_m was recorded in I=0 mode within 5 s of achieving the whole-cell configuration. To monitor the continuous V_m in individual cells in response to pharmacological treatments, cells were held in the whole-cell configuration for 6 min, with 60 s in the standard PSS, followed by 150 s in treatment and a further 150 s for washout of treatment. Where relevant, a vehicle treatment control was included in each experiment. The mean V_m over the last 5 s in each of the three stages was used to compare the V_m data. The V_m signals were sampled at 200 Hz. Liquid junction potentials were calculated using the integrated tool in Clampex 10.4. Dose-response data were fitted to a sigmoidal logistic equation

$$\% \text{ block} = \frac{100}{1 + \left(\frac{IC_{50}}{[Drug]}\right)^n}$$

where IC₅₀ is the concentration of drug at which half of its maximal effect occurs; and *n* is the slope giving the Hill coefficient.

2.6 | Perforated patch clamp recordings

The perforated patch clamp technique was used to record K_{Ca}1.1 currents. The intracellular solution used in perforated patch recording contained (in mM) 5 choline-Cl, 145 KCl, 2 MgCl₂, 10 HEPES, and 1 EGTA adjusted to pH 7.4 with KOH. Nystatin (150 μM) in dimethyl sulfoxide was made up and added to the perforated patch intracellular solution on the day of the experiment. Typical series resistance ranged between 20 and 40 MΩ. K_{Ca}1.1 currents were elicited by depolarizing from –120 mV (250 ms) to voltages in the range –60 to +90 mV in 10 mV increments (300 ms). The outward current data were fitted to a single exponential decay (Sanguinetti & Jurkiewicz, 1990)

$$Y = Y_0 \times e^{kx}$$

where *k* is the rate constant.

2.7 | Intracellular Na⁺ and Ca²⁺ imaging

Measurement of [Na⁺]_i was performed as described in (Roger et al., 2007) with minor modifications. Briefly, 6 × 10⁴ cells grown on glass coverslips for 24 hr were labeled with 5 μM SBFI-AM (Sigma) and 0.1% v/v Pluronic F-127 (Life Technologies) in DMEM with 0% FBS at 37°C in the dark for 1 hr. Excess SBFI-AM was washed out with 37°C DMEM supplemented with 5% FBS. The coverslip was assembled into a RC-20H closed bath imaging chamber (Warner Instruments) and observed at room temperature using a Nikon Eclipse TE200 epifluorescence microscope at 40×. SBFI was alternately excited at 340 and 380 nm, and the fluorescence emission at 510 nm was collected at 8-bit depth using a Rolera-XR Fast 1394 CCD camera (QImaging) controlled by SimplePCI software (Hamamatsu). Calibration of [Na⁺]_i was performed after each recording by perfusing two solutions on the cells: 10 and 20 mM Na⁺. They contained (in mM) 149.4 NaCl + KCl, 1 MgCl₂, 2.5 CaCl₂, 5 HEPES, 5.6 glucose, and 0.02 gramicidin (Sigma), adjusted to pH 7.2 with KOH. In each experimental repeat, [Na⁺]_i of ≥ 7 individual cells in the field of view were calculated individually and then averaged. For Ca²⁺ imaging, cells were labeled with 1 μM Fura-2 AM (PromoKine) using the same procedure as above, with an additional wash step using 37°C phenol red-free DMEM (Life Technologies) after 1 hr incubation with the dye, and the images were captured at 20×. In each experimental repeat, the [Ca²⁺]_i of ≥ 17 individual cells in the field of view were measured. Each experiment was repeated at least three times.

2.8 | Western blot analysis

Western blot analysis was performed as described previously (Nelson et al., 2014). The primary antibodies were mouse anti-K_{Ca}1.1 (1:500; NeuroMab) and mouse anti-α-tubulin (1:10,000; Sigma).

2.9 | Cell migration assay

Cell migration was measured using wound healing assays (Yang et al., 2012). Label-free ptychographic microscopy was used to monitor

motility in real time (Marrison, Raty, Marriott, & O'Toole, 2013; Suman et al., 2016). Images were acquired over 16 hr at 9 min intervals using a Phasefocus VL-21 microscope with an 10× (0.25 NA) lens using 640 nm illumination and equipped with an environmental chamber maintaining the cells at 37°C in 5% CO₂. The wound healing experiment was repeated three times on separate days. Image sequences of gap closure were processed using Phasefocus Cell Analysis Toolbox (CAT) software to segment and track individual cells at the leading edge and measure wound area. For each image sequence, the following parameters were automatically measured: change in normalized gap area over time; $t_{1/2}$ for gap closure (hr), determined by applying a linear fit to the normalized wound area reduction from $t = 0$ until the time at which the area reduces by 50%; collective migration ($\mu\text{m/hr}$), defined as:

$$V_{\text{migration}} = \frac{|\text{slope}|}{2 \times l}$$

where slope is the rate of area of scratch closure and l is the length of the scratch; instantaneous velocity per cell ($\mu\text{m/s}$), considering segmented cells with track lengths of ≥ 5 frames; and directionality of leading-edge cells tracked for ≥ 5 frames, relative to the center of the scratch.

2.10 | Cell proliferation and invasion assays

Cell proliferation was measured using the thiazolyl blue tetrazolium bromide (MTT) assay, as described (Yang et al., 2012). Cell invasion was quantified using 24-well Corning BioCoat Matrigel Invasion Chambers according to the manufacturer's guidelines. Briefly, 2.5×10^4 MDA-MB-231 cells were seeded in the upper compartment supplemented with 1% FBS and appropriate treatments. The lower compartment contained 10% FBS and appropriate treatments. Cells were incubated at 37°C for 24 hr before the removal of non-invaded cells from the upper chamber using cotton buds. Cells that had invaded through the polyethylene terephthalate membrane were fixed using 4% paraformaldehyde for 10 min and were washed three times with phosphate buffered saline (PBS), 5 min/time, before staining with DAPI. The membrane was then mounted on a glass microscope slide. DAPI-positive cells on the membrane were viewed at 20× using a Nikon Eclipse TE200 epifluorescence microscope. Experiments were performed on duplicate wells and repeated ≥ 3 times.

2.11 | Immunocytochemistry

Cells (1.6×10^5) were cultured on glass coverslips in 4-well plates for 48 hr to form confluent monolayers. Wounds were made on the coverslip using a P200 pipette tip and debris was washed off with 37°C DMEM. Appropriate treatments were subsequently applied, and cells were allowed to migrate into the wound for 3 hr. This incubation duration was used because it was long enough to show an effect of V_m inhibition on migration. Cells were fixed in 4%

paraformaldehyde for 10 min and immunocytochemistry was performed, as described (Nelson et al., 2014). The following primary antibodies were used: rabbit anti-Na_v1.5 (1:100; Alomone); rabbit anti-K_{Ca}1.1 (1:100; Neuromab); mouse anti-Rac1-GTP (1:500; NewEast Biosciences); rabbit anti-total Rac1 (1:10; NewEast Biosciences); and mouse anti-CD44 (1:100; AbD Serotec). The secondary antibodies were Alexa 488 or 568-conjugated goat anti-mouse and Alexa 488 or 568-conjugated goat anti-rabbit (1:500; Life Technologies). In some experiments, cells were counter-stained with Alexa 633-conjugated phalloidin (1:50; Life Technologies). In experiments where permeabilized cells were labeled with Alexa 568-conjugated annexin V (1:20; Life Technologies), primary and secondary antibodies were incubated in Ca²⁺-containing annexin V binding buffer (Life Technologies) to preserve annexin V binding. Coverslips were then mounted on glass microscope slides using Prolong Gold with DAPI (Life Technologies). The slides were examined using a Zeiss LSM 710 confocal microscope at 40×. Confocal images were acquired sequentially for each channel. Images (512 × 512 or 1,024 × 1,024 pixels, dependent on experiment) were initially processed with the Zeiss Zen 2 software, and later exported into ImageJ for analysis. Brightness/contrast was adjusted using the ImageJ "Auto" function.

2.12 | Morphology and lamellipodium scoring

Circularity was calculated on manually segmented cells using the free-hand tool in ImageJ (Schneider, Rasband, & Eliceiri, 2012):

$$\text{Circularity} = 4\pi \times \frac{\text{Area}}{\text{Perimeter}^2}$$

Values approaching 0 indicate a more elongated cell morphology. Feret's diameter was measured as the maximum distance between any two points along the cell boundary. Three experimental repeats were performed, and 20–25 cells per condition were analyzed for every repeat. To score lamellipodia formation, cells were categorized into two groups: with and without lamellipodium. For each of the three experimental repeats, 40–50 cells per condition were analyzed blinded to treatment.

2.13 | Analysis of Rac1 localization in the lamellipodium

The signal densities of F-actin, Rac1-GTP and total Rac1 in the lamellipodium were analyzed in arcs at various distances from the leading edge as described (Dang et al., 2013). The region of interest in the lamellipodia was determined by the dense staining of F-actin. To avoid bias in choosing ROIs, the analysis was carried out blinded to treatment. The ImageJ Radial Profile Extended plugin (Philippe Carl, CNRS, France) was used with starting radius = 0.43 μm , radius increment = 0.43 μm , ending radius = 5.6 μm , and total integrated angle = 90°, resulting in 13 arcs in total. Signal densities on each of the arcs were obtained and were normalized to those on the innermost arc. Typically, 20–30 cells at the edge of the wound were

analyzed for each condition and the experiment was repeated three times.

2.14 | Colocalization analysis

Colocalization of annexin V and Rac1-GTP labeling within regions of interest drawn around the lamellipodium was evaluated using the Coloc2 plugin in ImageJ. The approximate point spread function on acquired images of $1,024 \times 1,024$ pixels was 2.71 pixels. For each region of interest, the thresholded Manders M1 and M2 coefficients for annexin V and Rac1-GTP were computed (Manders, Verbeek, & Aten, 1993), together with the Li's intensity correlation coefficient (Li et al., 2004). Measurements were taken from 30 cells per condition over three experimental repeats.

2.15 | In vitro Rac1 activity assay

Cells were cultured to 70% confluency in 6-well plates before addition of pharmacological treatment(s). After incubation for 24 hr, total cellular Rac1 activity was evaluated in cell lysates using a colorimetric ELISA-based small GTPase activation assay, according to the manufacturer's instructions (G-LISA; Cytoskeleton, Inc.; Antonov et al., 2012). Measurements were obtained from duplicate wells and the experiment was repeated three times.

2.16 | Live cell imaging of Rac1 biosensor activation

Cells (1.6×10^5) were cultured in 8-well chamber glass slides. After incubation for 24 hr, cells were transfected with 200 ng of a biosensor for Rac1 activation (pTriEx4-Rac1-2G; Addgene plasmid # 66110; Fritz et al., 2015) using Fugene (Roche; Nelson et al., 2014). Forty-eight hours following transfection, appropriate treatments in phenol red-free DMEM were applied for 3 hr before imaging. FRET imaging of biosensor activation was performed at room temperature using a Nikon Eclipse TE200 epifluorescence microscope with a 40 \times (NA 0.60) objective. Acquisition from cells expressing low levels of the biosensor was performed at 8-bit depth using a Rolera-XR Fast 1394 CCD camera (QImaging) controlled by SimplePCI software (Hamamatsu). Acquisition time for donor and FRET channels was typically 200 ms. The donor and acceptor channels were acquired sequentially. The donor, monomeric teal fluorescent protein (mTFP), was excited at 436 nm and emission was collected at 480 nm. FRET emission was collected above 540 nm. The acceptor (Venus) was excited at 480 nm and emission collected above 540 nm. Visualization of cells transfected with a control plasmid expressing mTFP alone, created by site-directed mutagenesis (Nelson et al., 2014), revealed minimal bleed-through in the FRET and Venus channels. Images were taken from ≥ 49 cells across three experimental repeats. Image processing was performed using ImageJ. Cells were manually segmented using the distribution of biosensor (donor mTFP signal). Images were then background subtracted before calculation of the FRET/mTFP integrated density ratio for each cell.

2.17 | Statistics

Data are presented as mean \pm standard error of mean (SEM). GraphPad Prism 7.0d was used to perform all statistical analyses. Polar histograms were plotted using OriginLab Origin 2017. For normally distributed data, paired or unpaired Student's two-tailed *t* test was used to compare two groups, as appropriate. Multiple comparisons were made using one-way analysis of variance (ANOVA) or repeated measures ANOVA followed by Tukey post hoc tests, as appropriate. For repeated measures data that were not normally distributed, a Friedman test with Dunn's post hoc tests was used. Fisher's exact test was used to examine the distribution of samples within a population. Contingency table data were analyzed using χ^2 test. Colocalization data were analyzed by two-way ANOVA. Results were considered significant at $p < .05$.

3 | RESULTS

3.1 | Na_v1.5 channels depolarize the membrane potential of breast carcinoma cells

The V_m of motile cancer cells is generally more depolarized than in terminally-differentiated noncancer cells (Yang & Brackenbury, 2013). In addition, both depolarized V_m and Na_v1.5 channel activity correlate with metastatic potential (Fraser et al., 2005). However, it is not known whether the relationship between Na_v1.5, V_m and cell behavior is causal. Here, we first investigated whether Na⁺ conductance through plasma membrane Na_v1.5 channels contributes to the depolarized V_m that has been reported previously in MDA-MB-231 cells (Fraser et al., 2005). Na_v1.5 carries a persistent inward Na⁺ current, small in amplitude compared with the transient Na⁺ current, which plays an important role in shaping the action potential firing pattern, especially in the subthreshold voltage range (George, 2005). In nonexcitable cells, this would allow significant accumulation of Na⁺ over an extended period, potentially permitting V_m depolarization at steady state. Na_v1.5 is robustly expressed in MDA-MB-231 cells, both in intracellular compartments and at the plasma membrane (Figure 1a). This agrees with previous reports of VGSC distribution in nonexcitable cells (Brisson et al., 2011, 2013; Carrithers et al., 2007, 2009; Fraser et al., 2005; Nelson, Yang, Millican-Slater et al., 2015; Persson et al., 2014; Yang et al., 2012). We measured Na⁺ currents carried by Na_v1.5 using whole-cell voltage-clamp recording. Depolarization from -120 mV to -10 mV elicited both transient and persistent inward Na⁺ currents (Figure 1b,c). Analysis of the voltage-dependent activation and steady-state inactivation of the Na⁺ current revealed a window current between -50 mV and -10 mV (Figure 1d,e). We next investigated whether Na_v1.5 could regulate the V_m . Stable suppression of Na_v1.5 expression using lentiviral shRNA (Nelson, Yang, Millican-Slater et al., 2015) significantly hyperpolarized the V_m compared with control cells, measured using whole-cell current-clamp recording, from -12.6 ± 0.9 mV to -16.0 ± 0.8 mV ($p < .01$; $n = 16$; *t* test; Figure 1f). Thus, Na_v1.5 is required to depolarize the steady-state V_m .

We next evaluated the effect of pharmacologically perturbing Na_v1.5 activity. The specific VGSC blocker TTX (30 μ M) reversibly inhibited the transient and persistent Na⁺ current ($p < .001$ and $p < .05$, respectively;

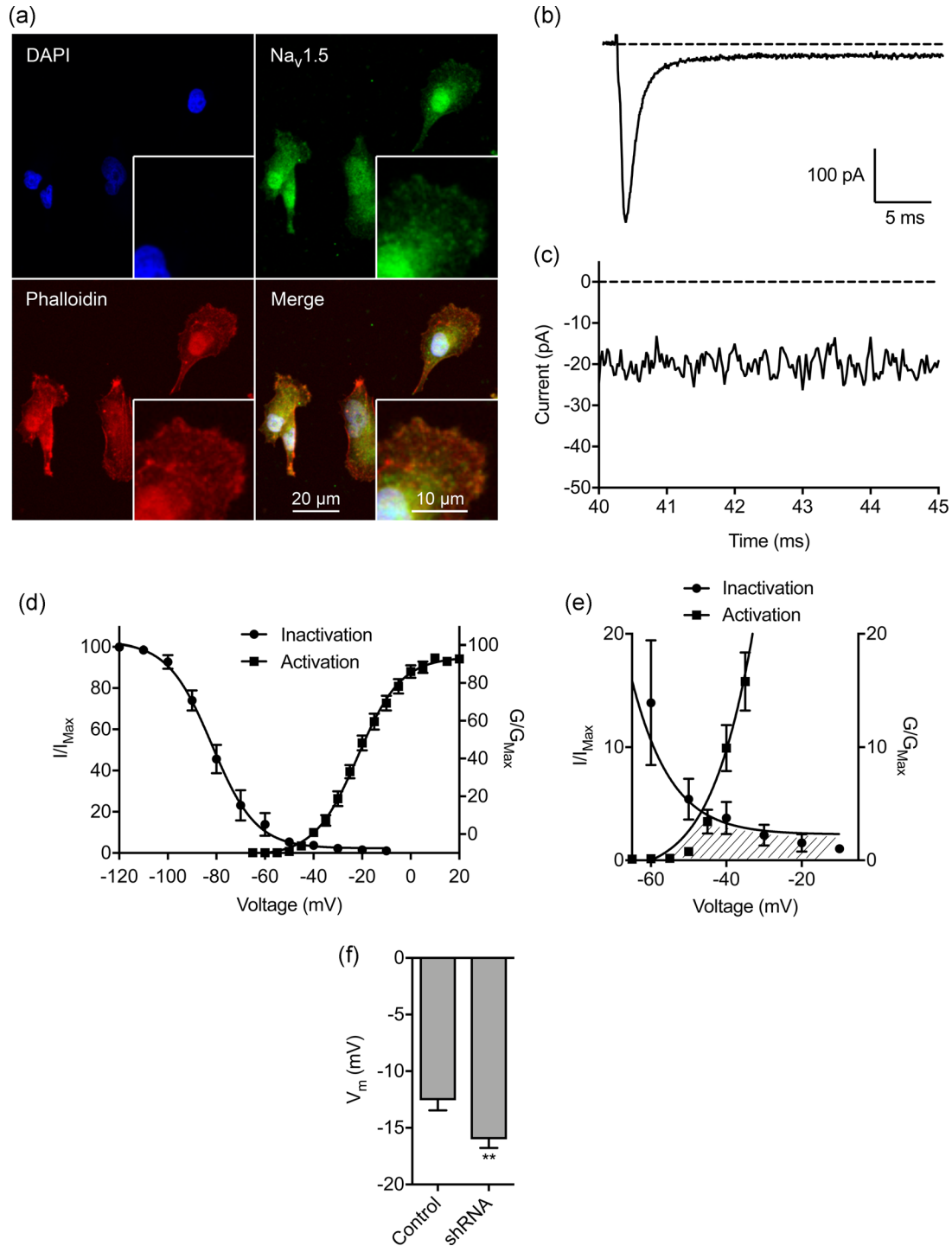


FIGURE 1 Na_v1.5 is endogenously expressed in breast carcinoma cells and regulates the membrane potential. (a) MDA-MB-231 cells labeled with Na_v1.5 antibody (green), phalloidin to label the actin cytoskeleton (red), and DAPI to label the nucleus (blue). Insets show cell peripheries at higher magnification. (b) Typical whole-cell recording showing large transient and small persistent Na⁺ current. The cell was depolarized to -10 mV for 50 ms following a 250 ms pre-pulse at -120 mV. (c) Expanded view of persistent Na⁺ current 40–45 ms following onset of depolarization. (d) Activation and steady-state inactivation of Na⁺ current. Normalized conductance (G/G_{Max}) was calculated from the current data and plotted as a function of voltage (n = 14). Normalized current (I/I_{Max}) was plotted as a function of the pre-pulse voltage (n = 9). Data are fitted with Boltzmann functions. (e) Expanded view of shaded area under activation and inactivation traces highlighting the window current. (f) Effect of Na_v1.5 shRNA knock-down on the V_m compared to nontargeting shRNA control (n = 16). Data are mean and SEM. *p < .05; **p < .01; Student's t test. DAPI, 4',6-diamidino-2-phenylindole; shRNA, short hairpin RNA

$n \geq 5$; repeated measures ANOVA with Tukey test; Figure 2a–d), consistent with previous reports (Brackenbury et al., 2007; Fraser et al., 2005; Roger et al., 2003). TTX also significantly hyperpolarized the V_m from -13.2 ± 1.3 mV to -17.5 ± 1.6 mV ($p < .01$; $n = 17$; repeated measures ANOVA with Tukey test; Figure 2e,f). On the other hand, the carrier for TTX (148 μ M sodium citrate, pH = 4.8) had no effect on the V_m (Figure S1a,b). In agreement with the TTX data, the VGSC-inhibiting antiepileptic drug, phenytoin (100 μ M) also significantly reduced the transient and persistent Na^+ current and hyperpolarized the V_m (Figure S1C–K). In contrast, veratridine (100 μ M), which increases channel open probability by inhibiting inactivation (Ulbricht, 1998), increased the persistent Na^+ current (Figure 2g,h; Figure S2a,b) and depolarized the V_m from -16.37 ± 1.4 mV to -12.6 ± 1.3 mV ($p < .05$; $n = 13$; t test; Figure 2h). In summary, these data show that pharmacological or genetic inhibition of $\text{Na}_v1.5$ hyperpolarizes the steady-state V_m , whereas increasing the persistent Na^+ current depolarizes the V_m . Thus, persistent current carried by $\text{Na}_v1.5$ contributes to V_m depolarization.

3.2 | Membrane potential depolarization is dependent on extracellular Na^+

To evaluate the sufficiency of extracellular Na^+ to determine the V_m , we next removed Na^+ in the extracellular solution during recording. Replacement of extracellular NaCl with choline chloride reversibly hyperpolarized the V_m from -10.4 ± 1.0 to -20.4 ± 2.0 mV ($p < .001$; $n = 10$; repeated measures ANOVA with Tukey test; Figure 3a,b). Using NMDG to replace extracellular Na^+ had a similar hyperpolarizing effect (Figure S2c,d). Thus, extracellular Na^+ is required for steady-state V_m depolarization.

Inward Na^+ current through $\text{Na}_v1.5$ channels would be expected to elevate the intracellular Na^+ level ($[\text{Na}^+]_i$) at steady state. Indeed, VGSCs have previously been shown to increase $[\text{Na}^+]_i$ (Campbell, Main, & Fitzgerald, 2013; Roger et al., 2007). We therefore next investigated the involvement of extracellular Na^+ in setting $[\text{Na}^+]_i$ using the ratiometric Na^+ indicator SBFI-AM (Figure 3c,d). Replacement of extracellular Na^+ with NMDG significantly reduced the steady-state $[\text{Na}^+]_i$ from 15.6 ± 1.7 mM to 7.6 ± 2.9 mM ($p < .001$; $n = 3$; ANOVA with Tukey test; Figure 3e). Treatment with TTX also significantly reduced the steady-state $[\text{Na}^+]_i$, suggesting that $\text{Na}_v1.5$ activity contributes to this elevation of $[\text{Na}^+]_i$ ($p < .05$; $n \geq 10$; ANOVA with Tukey test; Figure 3e). In agreement with this, the $[\text{Na}^+]_i$ of $\text{Na}_v1.5$ -shRNA cells was significantly lower than for control cells (9.4 ± 1.2 mM vs. 13.5 ± 0.6 mM; $p < .01$; $n = 3$; t test; Figure 3f). On the other hand, $\text{Na}_v1.5$ inhibition with TTX had no effect on $[\text{Ca}^{2+}]_i$ (Figure S3a–d). Together, these data suggest that Na^+ influx through $\text{Na}_v1.5$ channels increases $[\text{Na}^+]_i$, but not $[\text{Ca}^{2+}]_i$.

3.3 | $\text{K}_{\text{Ca}1.1}$ regulates the membrane potential but not the Na^+ level

$\text{Na}_v1.5$ channels enhance cell migration, invasion, tumor growth, and metastasis (Fraser et al., 2005; Nelson et al., 2015; Roger et al., 2003). Given that $\text{Na}_v1.5$ depolarizes the steady-state V_m , and that V_m

depolarization is functionally instructive in regulating cellular behavior (Yang & Brackenbury, 2013), we reasoned that $\text{Na}_v1.5$ may regulate cell migration via setting the V_m . Thus, we sought a means by which to manipulate the V_m independent of $\text{Na}_v1.5$ to separate the effects of V_m and $[\text{Na}^+]_i$ on downstream signaling. To do this, we took advantage of the ubiquitously expressed large conductance Ca^{2+} -activated K^+ channel, $\text{K}_{\text{Ca}1.1}$ (Contreras et al., 2013). We verified that $\text{K}_{\text{Ca}1.1}$ was robustly expressed in MDA-MB-231 cells (Khaitan et al., 2009; Ma et al., 2012; Roger, Potier, Vandier, Le Guennec, & Besson, 2004), and its expression was unaffected by $\text{Na}_v1.5$ downregulation (Figure 4a,b). Next, using the perforated patch clamp mode to maintain endogenous $[\text{Ca}^{2+}]_i$, we found that the $\text{K}_{\text{Ca}1.1}$ opener NS-1619 (1 μ M; Macmillan, Sheridan, Chilvers, & Patmore, 1995) increased outward K^+ current, confirming $\text{K}_{\text{Ca}1.1}$ activity (Figure 4c,d). Co-application of the $\text{K}_{\text{Ca}1.1}$ channel blocker iberiotoxin (100 nM) inhibited the potentiating effect of NS-1619 on the outward current (Figure 4c,d) confirming specificity of NS-1619. We next studied the effect of NS-1619 on the V_m . NS-1619 hyperpolarized the steady-state V_m in a dose-dependent manner (Figure 4e). Importantly, 1 μ M NS-1619 hyperpolarized the V_m by 4.4 mV from -10.6 ± 1.3 mV to -15.0 ± 0.6 mV ($p < .01$; $n \geq 12$; t test; Figure 4f). This shift is equivalent to the hyperpolarization elicited by inhibiting $\text{Na}_v1.5$ activity (Figure 2f,i). In contrast, NS-1619 treatment did not significantly alter the $[\text{Na}^+]_i$ ($p = .93$; $n = 22$; paired t test; Figure 4g) or $[\text{Ca}^{2+}]_i$ (Figure S3e,f). Finally, the V_m recorded using the standard intracellular solution (free $[\text{Ca}^{2+}] = 5.7$ nM) was not significantly different from that recorded using intracellular solution with 100 nM free $[\text{Ca}^{2+}]$ ($p = .82$; $n = 12$; t test; Figure 4h), suggesting that at physiological $[\text{Ca}^{2+}]_i$ (Sareen, Darjatmoko, Albert, & Polans, 2007; Winnicka, Bielawski, Bielawska, & Surazynski, 2008), $\text{K}_{\text{Ca}1.1}$ channels do not contribute to regulating the V_m in the absence of NS-1619. In summary, activation of $\text{K}_{\text{Ca}1.1}$ hyperpolarizes the V_m to the same extent as $\text{Na}_v1.5$ inhibition, thus providing an experimental means by which to manipulate the V_m independent of Na^+ .

3.4 | $\text{Na}_v1.5$ -dependent membrane potential depolarization regulates cell migration and morphology

Using NS-1619 and TTX as tools to modify the V_m independent of, or as a result of $\text{Na}_v1.5$ activity, respectively, we next investigated the effect of V_m depolarization on cell migration in wound healing assays using label-free ptychographic imaging (Figure 5a). Both TTX and NS-1619 slowed the rate of wound closure (Figure 5b). The $t_{1/2}$ of wound closure increased from 5.7 ± 1.1 hr to 9.8 ± 0.7 hr in the presence of TTX and 9.9 ± 0.1 hr in the presence of NS-1619 ($p < .05$; $n \geq 5$; ANOVA with Tukey test; Figure 5c). Similarly, the collective migration of cells moving into the wound was reduced from 7.8 ± 0.7 $\mu\text{m/hr}$ to 5.5 ± 0.4 $\mu\text{m/hr}$ in the presence of TTX and 4.9 ± 0.5 $\mu\text{m/hr}$ in the presence of NS-1619 ($p < .05$; $n \geq 5$; ANOVA with Tukey test; Figure 5d). The instantaneous velocity of individual cells at the leading edge was also reduced from $6.2 \times 10^{-3} \pm 5.6 \times 10^{-5}$ $\mu\text{m/s}$ to $4.7 \times 10^{-3} \pm 5.0 \times 10^{-5}$ $\mu\text{m/s}$ and $4.4 \times 10^{-3} \pm 4.5 \times 10^{-5}$ $\mu\text{m/s}$, for TTX- and NS-1619-treated cells, respectively ($p < .001$; $n \geq 2,662$; Kruskal–Wallis with Dunn's test; Figure 5e). In addition, both TTX and NS-1619 caused a small, but statistically

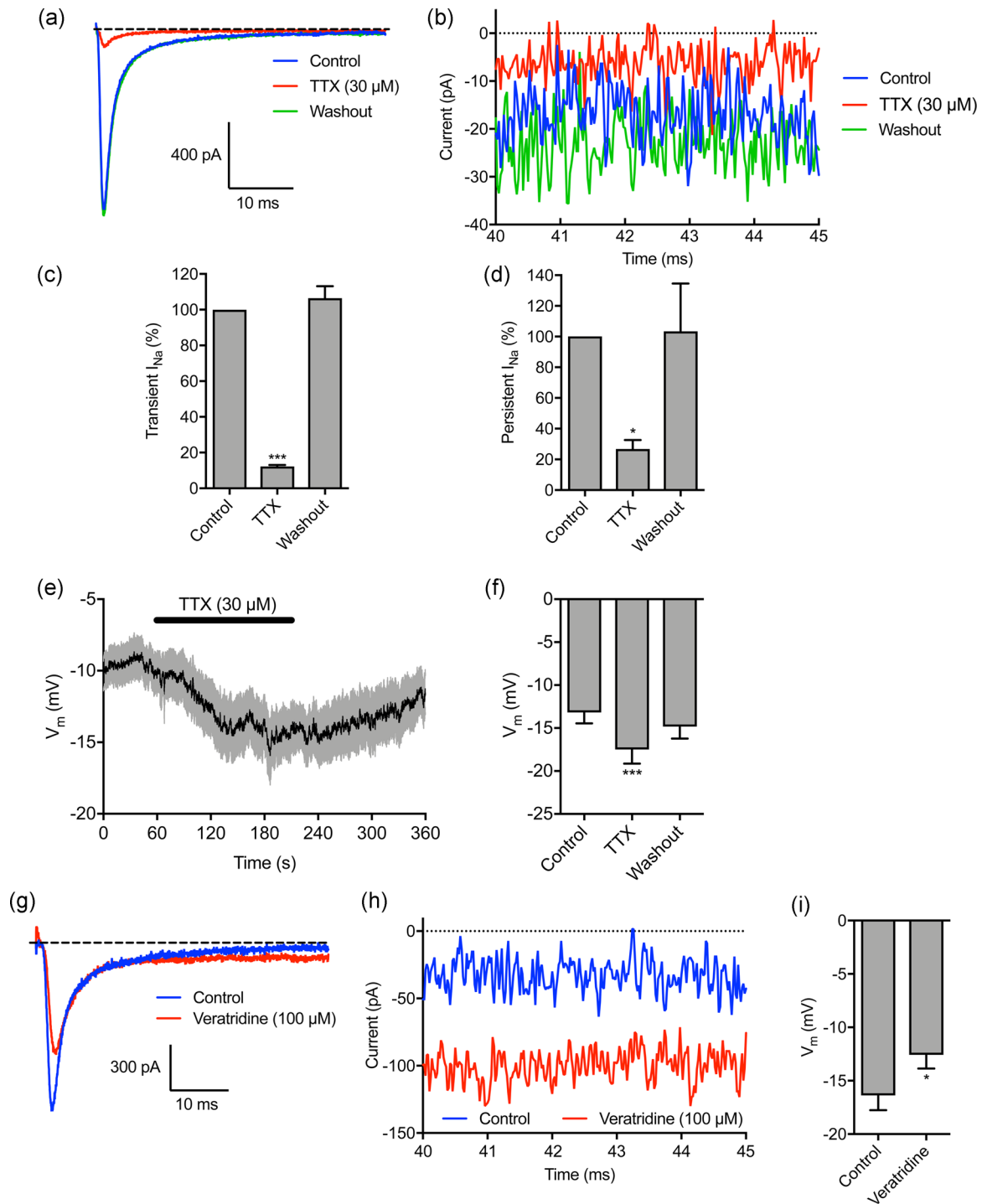


FIGURE 2 Tetrodotoxin hyperpolarizes, and veratridine depolarizes, the membrane potential. (a) Representative trace showing the inhibitory effect of tetrodotoxin (TTX; 30 μM) on Na⁺ current, and recovery after washout. The cell was held at -120 mV for 250 ms before depolarizing to -10 mV for 50 ms. (b) Expanded view of persistent Na⁺ current 40–45 ms following onset of depolarization. (c) Quantification of the normalized transient Na⁺ current after TTX (30 μM) treatment and following washout (n = 7). (d) Quantification of the normalized persistent Na⁺ current after TTX (30 μM) treatment and following washout (n = 4). (e) V_m in control physiological saline solution, after TTX (30 μM) treatment and following washout. Solid line, mean; gray shading, SEM (n = 17). (f) Quantification of V_m over the last 5 s in control, TTX, and washout (n = 17). (g) Representative trace showing effect of veratridine (100 μM) on Na⁺ current. The cell was held at -120 mV for 250 ms before depolarizing to 0 mV for 50 ms. (h) Expanded view of persistent Na⁺ current 40–45 ms following onset of depolarization. (i) V_m in control PSS and 120 s after perfusion with veratridine (n = 13). Data are mean and SEM. **p < .01; ***p < .001; repeated measures ANOVA with Tukey test for (c), (d), (f); Student's *t* test for (i). ANOVA, analysis of variance; PSS, physiological saline solution; SEM, standard error of mean

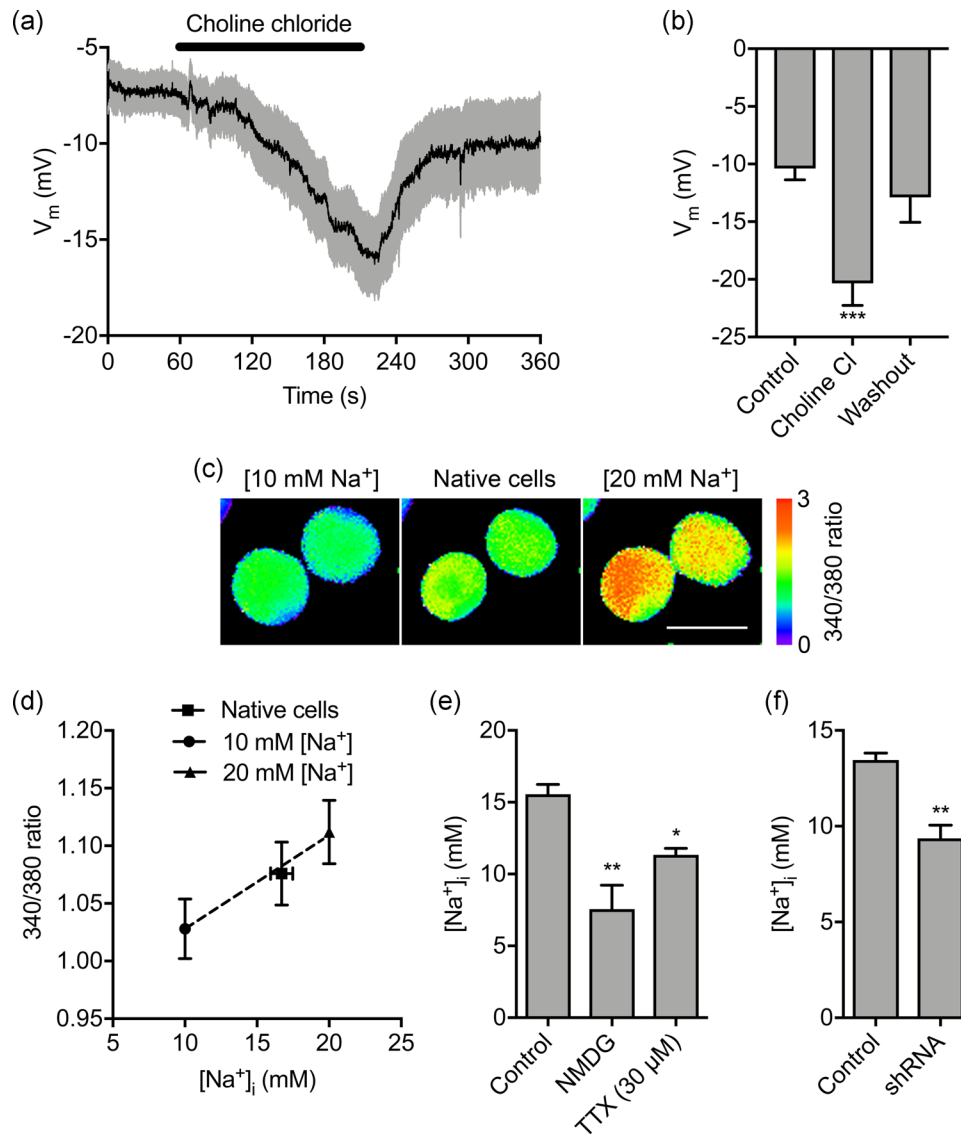


FIGURE 3 Extracellular Na⁺ sets the membrane potential and intracellular Na⁺ level. (a) V_m in control physiological saline solution, after extracellular Na⁺ replacement with choline chloride and following washout. Solid line, mean; gray shading, SEM ($n = 10$). (b) Quantification of V_m over the last 5 s in control, choline chloride, and washout ($n = 10$). (c) Representative SBF fluorescence intensity (ratio of emission at 340 nm/380 nm) when cells were perfused with standard physiological saline (center panel), solution containing 10 mM Na⁺ and 20 μ M gramicidin (left panel) and solution containing 20 mM Na⁺ and 20 μ M gramicidin (right panel). Ratio images are color-coded so that warm and cold colors represent high and low [Na⁺]_i, respectively. Scale bar = 10 μ m. (d) Calibration of relationship between SBF fluorescence intensity (340/380 ratio) and [Na⁺]_i. Dashed line, linear regression ($r^2 = 0.99$; $n = 40$). (e) Quantification steady-state [Na⁺]_i in control physiological saline solution ($n = 6$), when extracellular Na⁺ was replaced with NMDG ($n = 3$), and in TTX (30 μ M; $n = 3$). (f) Effect of Na_v1.5 shRNA knock-down on [Na⁺]_i compared with nontargeting shRNA control ($n = 3$). Data are mean and SEM. * $p < .05$; ** $p < .01$; *** $p < .001$; ANOVA with Tukey post hoc test for (a) and (e); Student's t test for (f). ANOVA, analysis of variance; NMDG, N-methyl-D-glucamine; SEM, standard error of mean; shRNA, short hairpin RNA; TTX, tetrodotoxin

significant, disruption in the directionality of cells at the leading edge, reducing the proportion of cells migrating directly into the wound ($p < .001$; Friedman with Dunn's test; Figure 5f). Hyperpolarizing the V_m with NS-1619 did not significantly alter cell proliferation measured in an MTT assay (Figure S4a). Given that inhibiting Na_v1.5 with TTX has no effect on the proliferation of MDA-MB-231 cells (Fraser et al., 2005; Gillet et al., 2009; Roger et al., 2003), together, these data suggest that both Na_v1.5 activity and V_m depolarization promote cellular migration, without affecting proliferation. On the other hand, whilst TTX

significantly reduced invasion into Matrigel, consistent with previous reports (Brackenbury et al., 2007; Driffort et al., 2014; Fraser et al., 2005; Nelson et al., 2015; Roger et al., 2003; Yang et al., 2012), NS-1619 had no effect (Figure S4b,c). Thus, Na_v1.5 promotes cellular migration via V_m depolarization, whereas Na_v1.5-dependent promotion of invasion occurs via a V_m -independent mechanism.

Na_v1.5 promotes an elongate, mesenchymal-like motile morphology (Brisson et al., 2013; Driffort et al., 2014; Nelson et al., 2015). This morphological modulation has been shown to occur through two

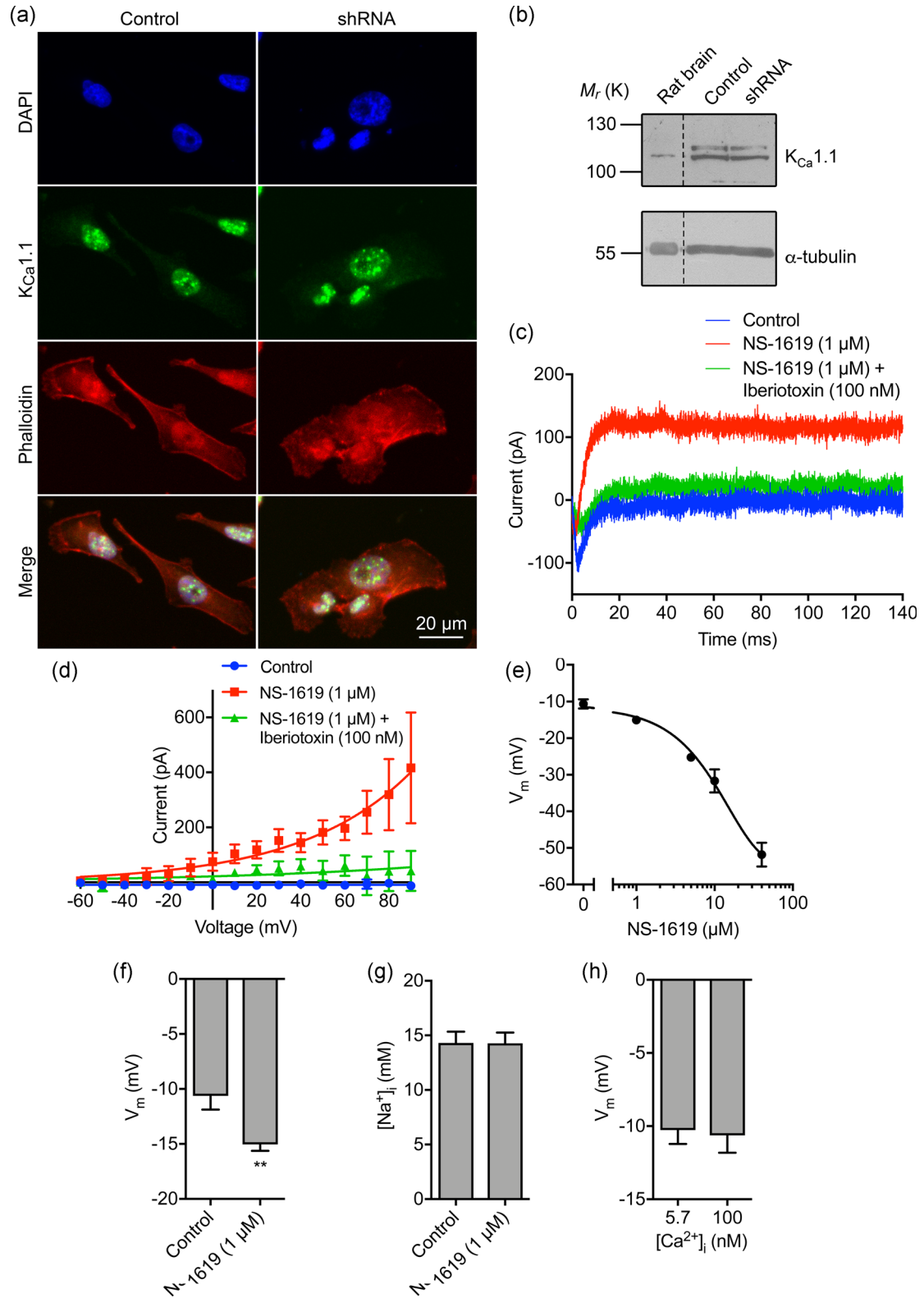


FIGURE 4 Continued.

potentially overlapping mechanisms: (a) regulation of adhesion-mediated signaling via $\beta 1$ subunits and upregulation of CD44 expression (Nelson et al., 2014, 2015), and (b) via increased Src kinase activity, phosphorylation of the actin-nucleation-promoting factor cortactin, and F-actin polymerization (Brisson et al., 2013). In addition, the V_m has been shown to promote reorganization of the actin filament network and cytoskeleton in other cell types (Chifflet et al., 2003, 2004, 2005; Nin et al., 2009; Szasz et al., 2005). However, the potential involvement of V_m in $Na_v1.5$ -mediated signaling is not known. We thus investigated the participation of $Na_v1.5$ -mediated V_m depolarization in regulating cell morphology. TTX (30 μ M) significantly increased cell circularity after 3 hr ($p < .001$; $n \geq 61$; ANOVA with Tukey test; Figure 6a,b) consistent with previously published data (Brisson et al., 2013). NS-1619 (1 μ M) also increased circularity ($p < .05$; $n \geq 61$; ANOVA with Tukey test; Figure 6a,b). Similarly, TTX and NS-1619 both significantly reduced the Feret's diameter (maximum caliper distance across the cell; $p < .01$; $n \geq 57$; ANOVA with Tukey test; Figure 6c). These data suggest that V_m depolarization promotes acquisition of an elongate phenotype.

Given that $Na_v1.5$ -mediated V_m depolarization promotes both morphological changes and cellular migration, we postulated that it might regulate formation of lamellipodia in migrating cells. We therefore scored the number of migrating cells with visible lamellipodia in a wound healing assay following treatment with TTX and NS-1619. Both treatments significantly reduced the proportion of cells with a lamellipodium in the measured population ($p < .001$; $n \geq 139$ cells per condition; χ^2 test; Figure 6d). Together, these findings suggest that $Na_v1.5$ -mediated V_m depolarization promotes a change in cellular morphology towards an elongate phenotype, and increases lamellipodia formation, thus potentiating cellular migration.

3.5 | $Na_v1.5$ -dependent membrane potential depolarization regulates Rac1 activation

The small GTPase Rac1, together with Rho and cdc42, plays a critical role in regulating cytoskeletal organization and cell motility (BurrIDGE & Wennerberg, 2004). In addition, Rac1 also regulates the formation of lamellipodia, cell motility and the directionality of cell movement (Wu et al., 2009). We therefore postulated that $Na_v1.5$ and V_m depolarization may regulate the level of active (GTP-bound) Rac1 in the lamellipodia of migrating cells. We treated migrating cells with

NS-1619 and TTX for 3 hr and then evaluated distribution of Rac1-GTP by quantifying immunocytochemical signal density across concentric arcs in the lamellipodium of individual cells (Figure 7a,b). As reported previously, a large quantity of Rac1 is present intracellularly in the perinuclear region, although there is also an enrichment of Rac1-GTP in the lamellipodium, consistent with its critical role in this region (Garcia-Mata et al., 2011; Wu et al., 2009). Both TTX and NS-1619 significantly reduced the peak Rac1-GTP signal at the leading edge of migrating cells ($p < .05$; $n \geq 66$; one-way ANOVA with Tukey test; Figure 7c). However, the level of total cellular Rac1-GTP, determined in whole-cell lysates, was unaffected by TTX treatment ($p = .80$; $n = 6$; t test; Figure 7d). Given that the majority of Rac1 is present intracellularly (Figure 7a; Das et al., 2015; Moissoglu, Slepchenko, Meller, Horwitz, & Schwartz, 2006), these data suggest that $Na_v1.5$ may regulate Rac1 locally at the plasma membrane and/or within lamellipodia. We next evaluated the effect of TTX and NS-1619 on distribution of Rac1-GTP versus total Rac1 using an antibody that does not distinguish between GDP- and GTP-bound forms of Rac1 (Figure 7e). The peak total Rac1 signal at the leading edge of migrating cells was unaffected by both TTX and NS-1619 ($p = .69$; $n \geq 60$; one-way ANOVA; Figure 7f,g). Thus, the ratio of peak Rac1-GTP to total Rac1 at the leading edge was significantly reduced by both TTX and NS-1619 ($p < .001$; $n = 3$; one-way ANOVA; Figure 7h). These data suggest that V_m depolarization caused by steady state $Na_v1.5$ activity increases Rac1 activation at the leading edge of migrating cells.

V_m depolarization promotes clustering and activation of the small GTPase K-Ras as a result of voltage-dependent redistribution of charged phospholipids including phosphatidylserine (Zhou et al., 2015). Given that Rac1 is also anchored to the inner leaflet of the plasma membrane via interaction with phosphatidylserine (Finkielstein et al., 2006; Magalhaes & Glogauer, 2010), we reasoned that a similar voltage-dependent mechanism may be responsible for Rac1 activation in the lamellipodia. We therefore next evaluated the effect of V_m depolarization on colocalization of Rac1-GTP with phosphatidylserine, using annexin V as a marker (Figure 8a). Treatment of migrating cells with TTX and NS-1619 reduced colocalization of Rac1-GTP with phosphatidylserine in the lamellipodia (Figure 8b-d). This was confirmed by quantification of thresholded Manders colocalization coefficients for phosphatidylserine and Rac1-GTP ($p < .01$; $n = 30$; two-way ANOVA with Tukey test; Figure 8e). Similarly, the TTX and NS-1619 treatments both reduced the Li's

FIGURE 4 The large conductance Ca^{2+} -activated K^+ channel $K_{Ca}1.1$ regulates the membrane potential but not intracellular Na^+ . (a) MDA-MB-231 cells labeled with $K_{Ca}1.1$ antibody (green), phalloidin to label the actin cytoskeleton (red), and DAPI to label the nucleus (blue). (b) Western blot of $K_{Ca}1.1$ in control MDA-MB-231 cells and cells in which $Na_v1.5$ has been knocked down with shRNA. Positive control = rat brain lysate. Loading control = α -tubulin. (c) Representative perforated patch clamp recording showing activation of outward current using the $K_{Ca}1.1$ activator (NS-1619; 1 μ M) and inhibition with iberiotoxin (100 nM). The cell was held at -120 mV for 250 ms before depolarization to $+60$ mV for 300 ms. (d) Current-voltage relationship of the $K_{Ca}1.1$ current. Cells were held at -120 mV for 250 ms before depolarization to voltages ranging from -60 to $+90$ mV in 10 mV steps for 300 ms ($n = 5$). Data are fitted with single exponential functions. (e) Dose-dependent effect of NS-1619 on the steady-state V_m ($n \geq 6$). Data are fitted to a sigmoidal logistic function. (f) Effect of NS-1619 (1 μ M) on steady-state V_m ($n = 12$). (g) Effect of NS-1619 (1 μ M, 5 min) on $[Na^+]_i$ ($n = 22$). (h) V_m recorded using intracellular solution with free $[Ca^{2+}]_i$ buffered to 5.7 nM versus 100 nM ($n \geq 10$). Data are mean and SEM. $**p < .01$; Student's paired t test. DAPI, 4',6'-diamidino-2-phenylindole; shRNA, short hairpin RNA

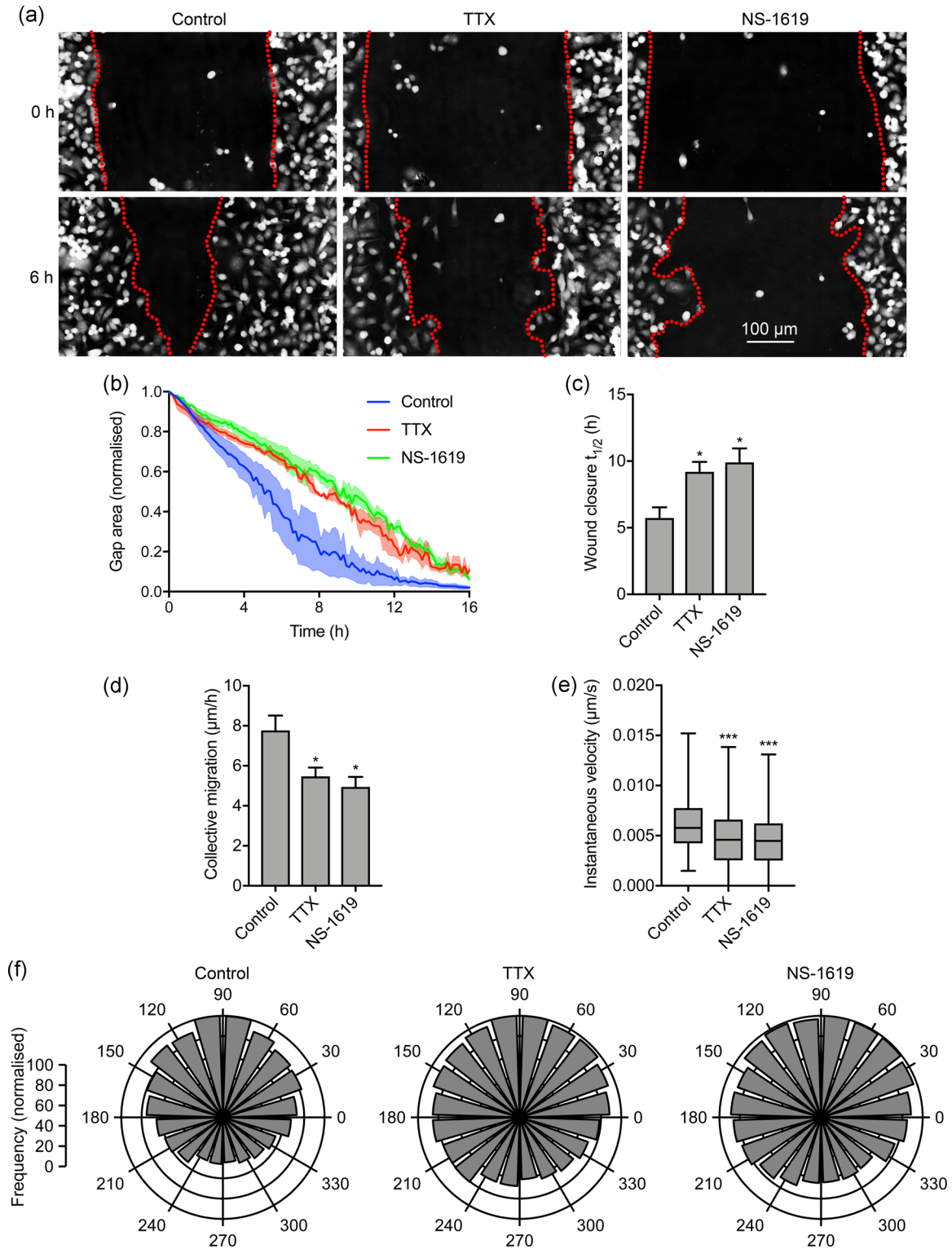


FIGURE 5 $\text{Na}_v1.5$ -dependent membrane potential depolarization regulates cell migration. (a) Representative scratch wounds at 0 hr and 6 hr into a wound healing assay \pm TTX (30 μ M) or NS-1619 (1 μ M). Red dotted lines highlight wound edges. (b) Wound area during the migration assay ("gap remaining"), normalized to starting value ($n = 3$). (c) $t_{1/2}$ of wound closure ($n \geq 5$). (d) Collective migration (μ m/hr) of cells closing the wound ($n \geq 5$). (e) Instantaneous velocity (μ m/s) of segmented cells ($n \geq 2,662$). (f) Polar histograms showing directionality of migrating cells at the leading edge of wounds ($p < .001$; Friedman with Dunn's test). 90° = axis perpendicular to wound. Data in (b-d) are mean and SEM. Box plot whiskers in (e) show maximum and minimum values and horizontal lines show 75th, 50th, and 25th percentile values. $*p < .05$; $**p < .01$; $***p < .001$; ANOVA with Tukey test (c, d); Kruskal-Wallis with Dunn's test (e). ANOVA, analysis of variance; SEM, standard error of mean; TTX, tetrodotoxin

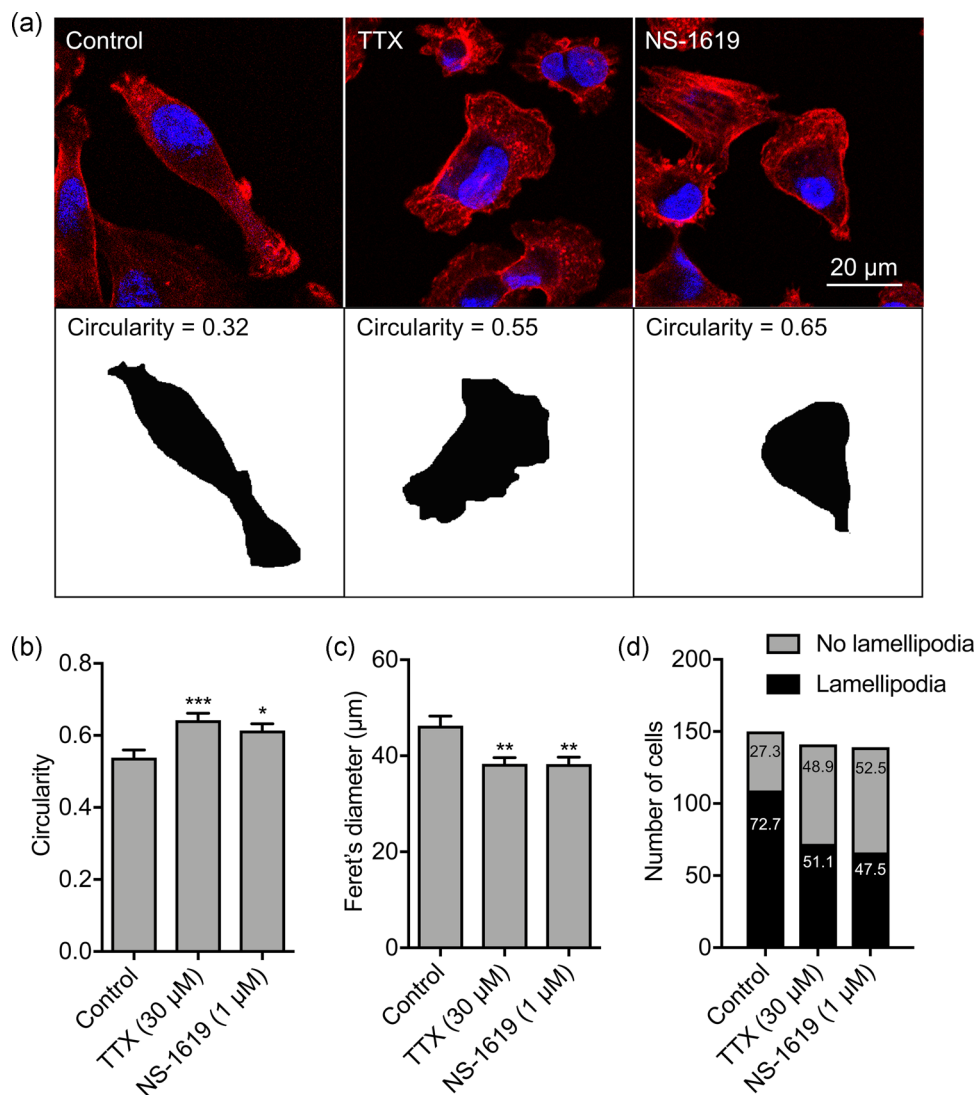


FIGURE 6 $\text{Na}_v1.5$ -dependent membrane potential depolarization regulates lamellipodia formation. (a) Images of representative cells after treatment with TTX (30 μM) or NS-1619 (1 μM) for 3 hr. Cells were fixed and stained with phalloidin (red) and DAPI (blue). Lower row shows masks of cells in the upper row, from which the circularity was calculated. (b) Circularity ($n \geq 61$). (c) Feret's diameter (μm ; $n \geq 57$). (d) Number of MDA-MB-231 cells with a lamellipodium ($p < .001$; χ^2 test). Numbers in bars are %. Bars in (b) and (c) are mean and SEM. * $p < .05$; ** $p < .01$; *** $p < .001$; ANOVA with Tukey test. ANOVA, analysis of variance; DAPI, 4',6-diamidino-2-phenylindole; SEM, standard error of mean; TTX, tetrodotoxin

intensity correlation quotient ($p < .001$; $n = 30$; one-way ANOVA with Tukey test; Figure 8f). These data support the notion that V_m depolarization increases Rac1 localization in the lamellipodia as a result of its interaction with phosphatidylserine.

To evaluate whether $\text{Na}_v1.5$ -mediated V_m depolarization promotes Rac1 activity in live cells, and to independently confirm the immunocytochemistry data, we next employed a genetically encoded Rac1 FRET biosensor to monitor Rac1 activation. In agreement with a previous report (Fritz et al., 2015), the biosensor showed a general gradient of Rac1 activation increasing from the cell interior towards the periphery, consistent with its critical role in actin remodeling at the edge of migrating cells (Figure 9a; Wu et al., 2009). Treatment with TTX did not affect biosensor distribution (Figure 9a), but suppressed activation at the periphery (Figure 9b,c). Quantification of FRET across

the whole cell revealed that TTX significantly reduced Rac1 activation to $48.6 \pm 5.2\%$ of control ($p < .001$; $n \geq 49$; t test; Figure 9d). Together, these results indicate that blockade of $\text{Na}_v1.5$ channels suppresses Rac1 activation at the cell periphery.

3.6 | $\text{Na}_v1.5$ -mediated morphological changes are dependent on Rac1 activation

Given that $\text{Na}_v1.5$ -dependent V_m depolarization promotes morphological changes leading to increased cell migration (Figures 5,6), and that $\text{Na}_v1.5$ promotes activation of Rac1 (Figures 7,8,9), which in turn, plays a key role in regulating cellular morphology and migration (Wu et al., 2009), we analyzed the impact of Rac1 inhibition on $\text{Na}_v1.5$ -dependent changes in cell morphology (Figure 10a). The specific Rac1 inhibitor

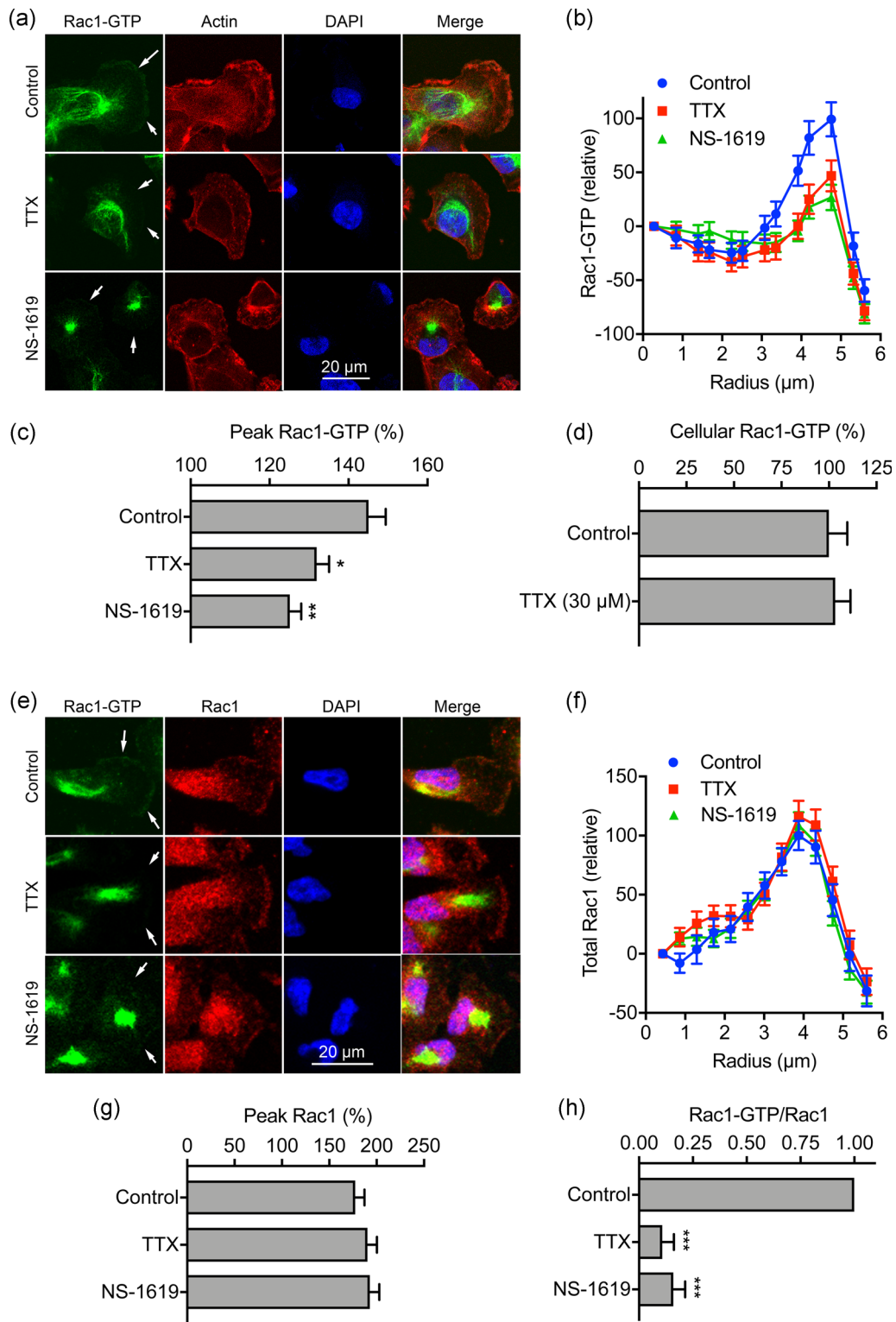


FIGURE 7 Continued.

EHT1864 increased circularity and reduced Feret's diameter in a dose-dependent manner (Figure S5a,b). Furthermore, EHT1864 increased circularity to a similar extent to TTX ($p < .001$; $n \geq 308$; one-way ANOVA with Tukey test; Figure 10b,c). Importantly, co-application of EHT1864 with TTX had no additive effect on circularity or Feret's diameter (Figure 10b,c). These results show that Rac1 activity is required to transduce the $\text{Na}_v1.5$ -dependent V_m depolarizing signal to promote acquisition of an elongate, motile cell phenotype (Figure 10d).

4 | DISCUSSION

Here we identify $\text{Na}_v1.5$ -mediated V_m depolarization as a regulator of Rac1 activation. Thus, we link ionic and electrical signaling at the plasma membrane to small GTPase-dependent cytoskeletal reorganization and cellular migration. We show that depletion of extracellular Na^+ or blockage of $\text{Na}_v1.5$ channels reversibly hyperpolarizes the V_m at the timescale of minutes. We further show that $\text{Na}_v1.5$ -dependent V_m depolarization increases Rac1 colocalization with phosphatidylserine at the leading edge of migrating cells, promoting Rac1 activation, and resulting in acquisition of a motile, mesenchymal-like cellular phenotype. We therefore propose that $\text{Na}_v1.5$ may serve as a sensor for local changes in the ionic microenvironment, thus permitting voltage-dependent activation of Rac1 to fine tune cell migration.

4.1 | Ion conductance, membrane potential, and migration

We show that $\text{Na}_v1.5$ carries a persistent inward Na^+ current in MDA-MB-231 cells. In agreement with the work of others, we report incomplete inactivation of $\text{Na}_v1.5$ resulting in a small voltage window encompassing the V_m , thus supporting this persistent Na^+ current (Brisson et al., 2011; Djamgoz & Onkal, 2013; Gillet et al., 2009; Nelson et al., 2015; Roger et al., 2003; Yang et al., 2012). The persistent inward Na^+ current carried by $\text{Na}_v1.5$ contributes to steady-state V_m depolarization. Our findings agree with another study in H460 non-small cell lung cancer cells, in which $\text{Na}_v1.7$ channels were shown to depolarize the V_m by ~ 10 mV (Campbell et al., 2013). Thus, the mechanism identified here is likely applicable to other nonexcitable cell types where VGSCs are expressed (Chen et al., 2019; Grimes et al., 1995; House et al., 2010;

Persson et al., 2014; Zhou et al., 2015). In addition, it has previously been shown that VGSCs contribute to steady-state V_m depolarization and viability in rat optic nerve axons and spinal cord astrocytes over a time course of hours (Sontheimer, Fernandez-Marques, Ullrich, Pappas, & Waxman, 1994; Stys, Sontheimer, Ransom, & Waxman, 1993), suggesting that this mechanism persists over an extended period. There may be other Na^+ -permeable pathway(s) also contributing to V_m regulation in nonexcitable cells, for example, via epithelial Na^+ channels (Amara, Ivy, Myles, & Tiriveedhi, 2016), Na^+ - K^+ ATPase (Winnicka et al., 2008), and NHE1 (Brisson et al., 2011). The V_m may also be dependent on the activity of transporters and channels regulating the movement of other ions, including Cl^- and K^+ (Yang & Brackenbury, 2013). The depolarized resting V_m reported here may therefore be attributed not only to the high permeability to Na^+ but also to the low expression/activity of hyperpolarizing K^+ channels.

Relatively small alterations in V_m can be functionally significant. For example, during synaptic transfer from photoreceptors to ganglion cells in turtle retina, V_m depolarizations as small as 5 mV are sufficient to activate paired ganglion cells (Baylor & Fettiplace, 1977). The V_m can function as an instructive signal to regulate cell cycle progression in proliferating cells (Cervera et al., 2016; Cone, 1971; Cone & Cone, 1976; Zhou et al., 2015). V_m depolarization can regulate other cellular behaviors, including differentiation (Sundelacruz et al., 2008) and cytoskeletal reorganization (Chifflet et al., 2003, 2004, 2005; Nin et al., 2009; Szaszi et al., 2005). At the tissue level, changes in V_m can also regulate morphogenesis, regeneration and tumorigenesis (Beane et al., 2011, 2013; Cervera et al., 2016; Chernet & Levin, 2014; Chernet et al., 2016; Lobikin et al., 2012, 2015). Several studies have shown that epithelial cells undergo V_m depolarization when migrating into wounds (Chifflet et al., 2004, 2005). However, an interesting and novel finding of our study here is that V_m depolarization is not simply a consequence of motile behavior (Schwab et al., 2012), but is itself a master regulator of morphological changes and migration. Here, we found that hyperpolarizing the V_m by ~ 5 mV reduced migration by $\sim 30\%$. The fact that this level of V_m hyperpolarization did not completely inhibit migration raises the possibility that additional hyperpolarization may have a further inhibitory effect. It is also likely that other ion conductance routes contributing to, and/or dependent on the V_m , may be involved in migration regulation. For

FIGURE 7 $\text{Na}_v1.5$ and V_m regulate Rac1 activation/distribution. (a) Images of representative cells after treatment with TTX (30 μM) and NS-1619 (1 μM) for 3 hr. Cells were labeled with Rac1-GTP antibody (green), phalloidin (red), and DAPI (blue). Arrows in the Rac1-GTP panels highlight the distribution or lack of expression at the leading edge. (b) Rac1-GTP signal density, measured across 20 arcs, in 0.43 μm radius increments, within a quadrant mask region of interest at the leading edge, normalized to the first arc ($n \geq 66$). (c) Peak Rac1-GTP signal density per cell from (b), normalized to the first arc ($n \geq 66$). (d) Total Rac1-GTP quantified in whole-cell lysates using colorimetric small GTPase activation assay ($n = 6$). (e) Images of representative cells after treatment with TTX (30 μM) and NS-1619 (1 μM) for 3 hr. Cells were labeled with Rac1-GTP antibody (green), total Rac1 antibody (red), and DAPI (blue). Arrows in the Rac1-GTP panels highlight the distribution or lack of expression at the leading edge. (f) Total Rac1 signal density, measured across 20 arcs, in 0.43 μm radius increments, within a quadrant mask region of interest at the leading edge, normalized to the first arc ($n \geq 59$). (g) Peak Rac1 signal density per cell from (f), normalized to the first arc ($n \geq 59$). (h) Ratio of Peak Rac1-GTP/Peak total Rac1 for each experimental repeat, normalized to control ($n = 3$). Data are mean and SEM. * $p < .05$; ** $p < .01$; *** $p < .001$; ANOVA with Tukey test. ANOVA, analysis of variance; DAPI, 4',6-diamidino-2-phenylindole; SEM, standard error of mean; TTX, tetrodotoxin

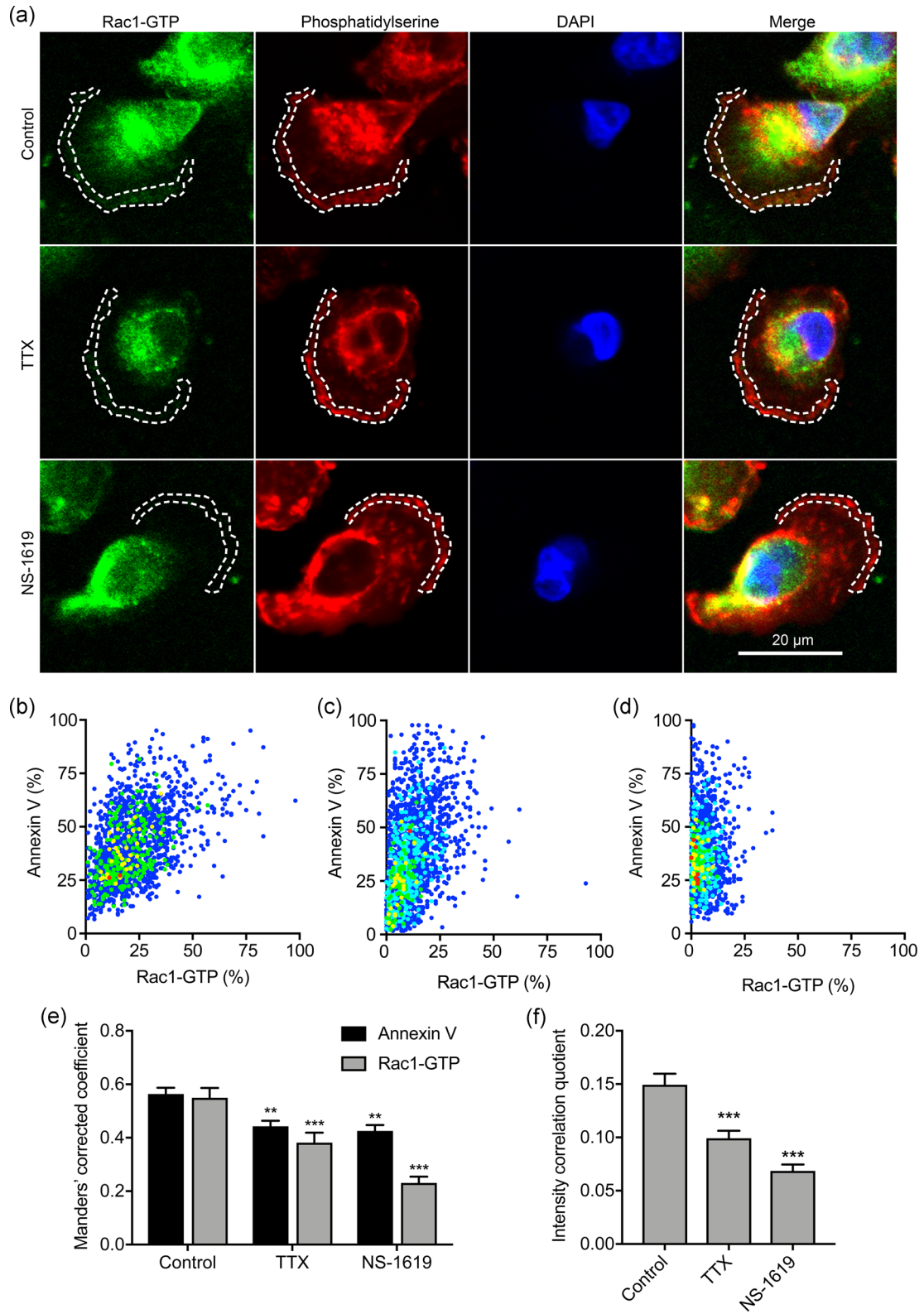


FIGURE 8 Continued.

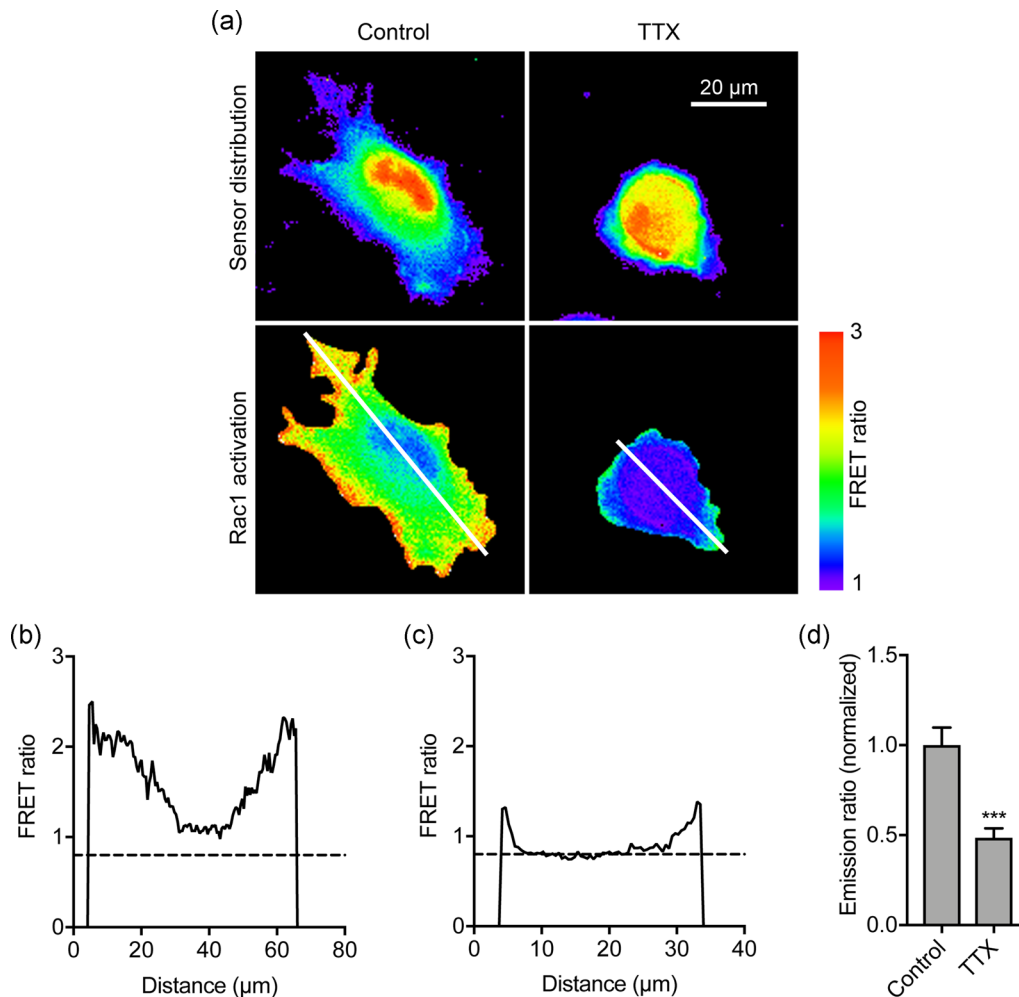


FIGURE 9 $\text{Na}_v1.5$ regulates Rac1 activation in live cells detected using a genetically encoded Rac1 FRET biosensor. (a) Images of representative cells after treatment \pm TTX ($30 \mu\text{M}$) for 3 hr. Rac1 activation biosensor distribution is shown in the donor (mTFP) channel. Images are color-coded so that warm and cold colors represent high and low values, respectively, for sensor distribution and activation (FRET). (b) Fluorescence intensity profile along line drawn across control cell in (a). (c) Fluorescence intensity profile along line drawn across TTX-treated cell in (a). (d) Emission ratio (FRET), for cells measured after treatment \pm TTX ($30 \mu\text{M}$) for 3 hr, normalized to control ($n \geq 33$). Data are mean and SEM. $**p < .01$; Student's *t* test. TTX, tetrodotoxin

example, hyperpolarization would increase the driving force for Ca^{2+} entry. Nonetheless, our data underscore that persistent Na^+ influx through $\text{Na}_v1.5$ channels leads to V_m depolarization, which in turn promotes cell migration.

Given the general trend towards depolarized V_m both in cancer cells (Cervera et al., 2016; Fraser et al., 2005; Yang & Brackenbury, 2013), and in epithelial cells undergoing migration (Chifflet et al.,

2004, 2005), we propose that voltage-dependent migratory behavior may be a general cellular phenomenon. For example, although involvement of V_m was not directly investigated, activation of the V_m -hyperpolarizing channel $\text{K}_{\text{Ca}1.1}$ with NS-1619 reduces migration of glioma cells (Kraft et al., 2003). Furthermore, VGSCs have been detected in cells from a broad range of tumor types, where they potentiate migration and invasion (Besson et al., 2015; Brackenbury,

FIGURE 8 $\text{Na}_v1.5$ and V_m regulate Rac1-GTP colocalization with phosphatidyserine. (a) Images of representative cells after treatment with TTX ($30 \mu\text{M}$) and NS-1619 ($1 \mu\text{M}$) for 3 hr. Cells were labeled with Rac1-GTP antibody (green), annexin V (red), and DAPI (blue). Dashed lines highlight regions of interest at the leading edge. (b) Cytofluorogram showing colocalization of annexin V and Rac1-GTP staining in region of interest in control cell from (a), normalized to maximum in each channel. (c) Cytofluorogram showing colocalization of annexin V and Rac1-GTP staining in region of interest in TTX cell from (a), normalized to maximum in each channel. (d) Cytofluorogram showing colocalization of annexin V and Rac1-GTP staining in region of interest in NS-1619 cell from (a), normalized to maximum in each channel. (e) Manders' corrected colocalization coefficients for annexin V and Rac1-GTP staining in regions of interest of cells after treatment with TTX ($30 \mu\text{M}$) and NS-1619 ($1 \mu\text{M}$) for 3 hr ($n = 30$). (f) Li's intensity correlation quotient for Rac1-GTP and annexin V colocalization ($n = 30$). Data are mean and SEM. $**p < .01$; $***p < .001$; ANOVA with Tukey test. ANOVA, analysis of variance; DAPI, 4',6-diamidino-2-phenylindole; SEM, standard error of mean; TTX, tetrodotoxin

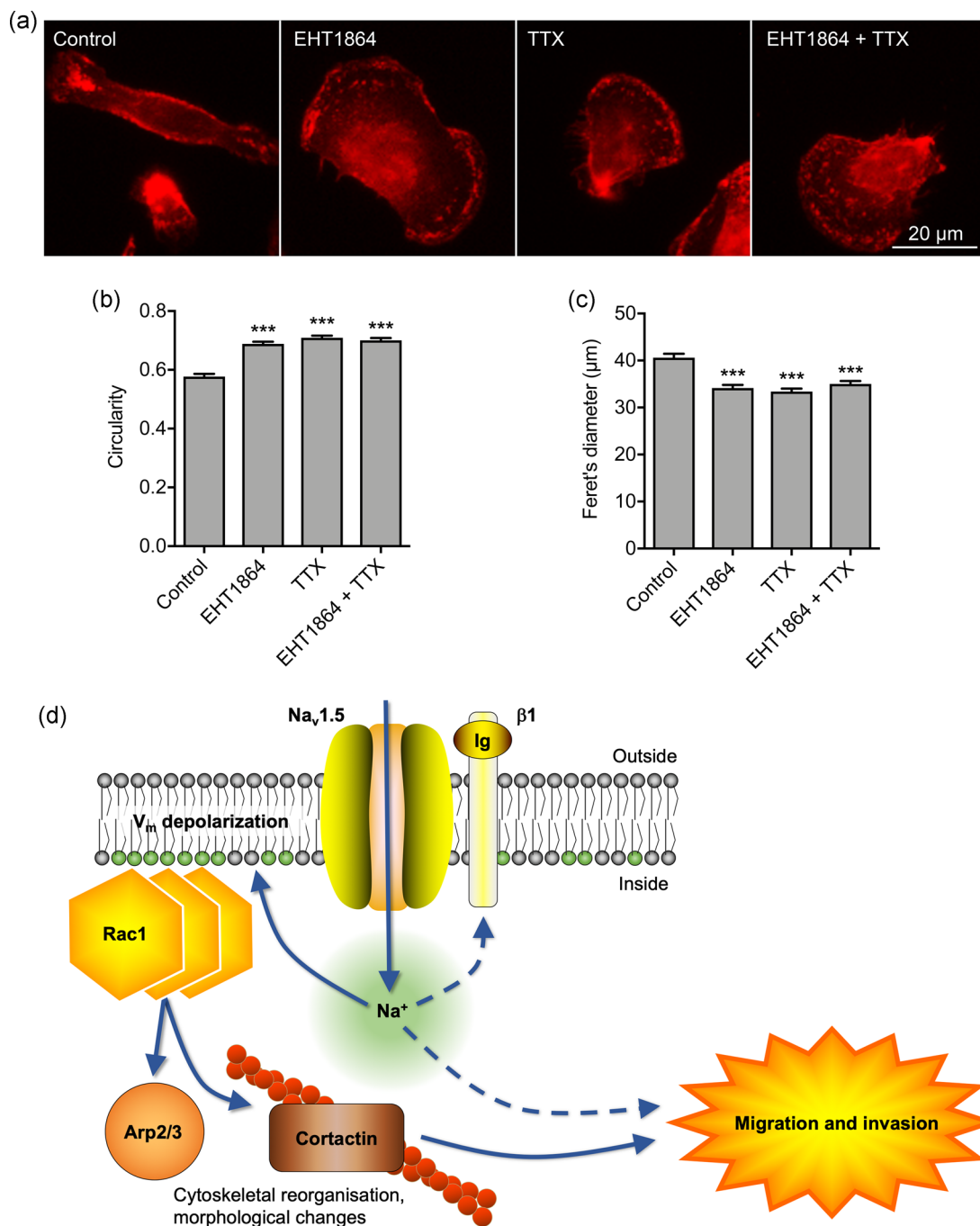


FIGURE 10 Na_v1.5-mediated morphological changes and migration are dependent on Rac1 activation. (a) Images of representative cells after treatment with TTX (30 μM) ± Rac1 inhibitor (EHT1864; 0.5 μM) for 3 hr. Cells are labeled with CD44 antibody (red). (b) Circularity of cells after treatment with TTX (30 μM) ± EHT1864 (0.5 μM) for 3 hr (n ≥ 308). (c) Feret's diameter (μm) of cells after treatment with TTX (30 μM) ± EHT1864 (0.5 μM) for 3 hr (n ≥ 308). Data are mean and SEM. ***p < .001; ANOVA with Tukey test. (d) Proposed mechanism underlying Na_v1.5-mediated V_m-dependent morphological changes and migration. Na_v1.5 channels carry Na⁺ influx, which depolarizes the V_m, causing redistribution of charged phosphatidylserine in the inner leaflet of the phospholipid bilayer, promoting Rac1 redistribution and activation. Rac1 regulates cytoskeletal modification via the Arp2/3 complex and increasing phosphorylation of cortactin and cofilin, promoting acquisition of a promigratory phenotype (Pollard, 2007; Stock & Schwab, 2015). Na⁺ influx through Na_v1.5 channels may also impact on migration and invasion through other mechanism(s), including via β1 subunit-dependent adhesion (Brisson et al., 2013; House et al., 2010, 2015; Nelson et al., 2014). ANOVA, analysis of variance; TTX, tetrodotoxin

2012). We therefore argue that the results presented here have broad applicability to other cell types.

4.2 | Voltage-dependent regulation of Rac1 activation

V_m depolarization promotes K-Ras clustering and subsequent activation (Zhou et al., 2015). Various small GTPases, including K-Ras and the Rho GTPases, are anchored to the inner leaflet of the plasma membrane through interaction with the anionic phospholipids PIP2, PIP3, and phosphatidylserine (Finkielstein et al., 2006; Heo et al., 2006; Magalhaes & Glogauer, 2010; Remorino et al., 2017; Zhou et al., 2015). In the case of K-Ras, clustering and activation has been shown using electron microscopy to arise as a result of depolarization-induced nanoscale redistribution of phosphatidylserine and PIP2 in the inner leaflet of the phospholipid bilayer, to which the K-Ras is anchored (Zhou et al., 2015). Our major discovery here is that Rac1 activation is also voltage-dependent. Our data show that $Na_v1.5$ -mediated V_m depolarization causes Rac1 activation, likely as a result of voltage-dependent redistribution of phosphatidylserine (Figure 10d). Thus, V_m -dependent signaling is not exclusively limited to mitogenic cascades but is also a key regulator of morphological changes and migration.

A growing body of evidence implicates V_m depolarization in regulation of small GTPase activity. For example, V_m has been shown to regulate the activity of GEF-H1, which, in turn, regulates the activity of the Rho/Rho kinase pathway (Waheed et al., 2010). V_m depolarization-dependent activation of Rho and subsequent cytoskeletal organization has been shown to be Ca^{2+} -independent (Szasz et al., 2005). In agreement with this, our data also imply that Ca^{2+} is not involved as a signaling intermediary in V_m depolarization-induced Rac1-mediated promotion of migration. On the other hand, in ATP-stimulated microglia, VGSC activity increases $[Ca^{2+}]_i$, and activates ERK and Rac1, promoting migration (Persson et al., 2014). V_m depolarization-induced activation of Ras and Rap1 has also been reported in mouse cortical neurons (Baldassa, Zippel, & Sturani, 2003).

The mechanism uncovered here may feed into, and interact with, additional signaling pathways which have been shown to be dependent on $Na_v1.5$ activity. For example, $Na_v1.5$ has been shown to promote Src kinase activity and phosphorylation of cortactin and cofilin (Brisson et al., 2013). Thus, $Na_v1.5$ -induced V_m depolarization may activate Rac1, increasing cortactin phosphorylation and therefore enhancing cofilin activity and actin filament polymerization. Src has also been shown to regulate Rac1 activity, suggesting the potential for feedback regulation (Servitja, Marinissen, Sodhi, Bustelo, & Gutkind, 2003). $Na_v1.5$ positively regulates the expression of the metastasis-promoting protein CD44, which may activate Src and therefore contribute to this process (Bourguignon, Zhu, Shao, & Chen, 2001; House et al., 2010, 2015; Lee, Wang, Sudhir, & Chen, 2008; Nelson, Yang, Millican-Slater et al., 2015). In addition, $Na_v1.5$ is expressed on astrocytes where it regulates migration by promoting reverse Na^+ / Ca^{2+} exchange (Black, Dib-Hajj, Cohen, Hinson, & Waxman, 1998; Pappalardo, Samad, Black, & Waxman, 2014). Furthermore, $Na_v1.5$ is expressed on the endosome of macrophages, where it regulates

endosomal acidification (Carrithers et al., 2007). On the other hand, $Na_v1.6$ is expressed within macrophage podosomes, where it promotes invasion via intracellular Na^+ release (Carrithers et al., 2009). $Na_v1.5$ and $Na_v1.6$ are also expressed on microglia, where the latter has been shown to also regulate migration and cytokine release (Black, Liu, & Waxman, 2009). It remains unknown whether $Na_v1.5$ opening changes during migration and what the signals might be that would regulate such alterations; however, it has been shown that $Na_v1.5$ can be regulated by growth factors and hormone signaling, and is itself mechanosensitive (Beyder et al., 2010; Fraser et al., 2014). Together, these studies suggest that VGSCs may further regulate the behavior of nonexcitable cells via pathways in addition to the one identified here.

4.3 | Implications for our understanding of metastasis

We provide evidence that $Na_v1.5$ contributes to steady-state V_m depolarization, which in turn promotes V_m -dependent Rac1 activation, lamellipodial protrusion formation and cellular migration. These data are in agreement with the previously reported role for VGSCs in regulating morphology and migration of tumor cells (Brackenbury & Djamgoz, 2006; Brackenbury et al., 2007; Brisson et al., 2013; Fraser, Ding, Liu, Foster, & Djamgoz, 1999; Fraser et al., 2005; Nelson et al., 2015). It is therefore conceivable that depolarization-dependent Rac1 activation may contribute to metastatic dissemination in response to local ionic changes in the tumor microenvironment. Thus, pharmacological targeting of VGSCs, which inhibits metastasis in preclinical models (Driffort et al., 2014; Nelson et al., 2015; Yildirim, Altun, Gumushan, Patel, & Djamgoz, 2012), may provide therapeutic benefit via V_m hyperpolarization and downregulation of V_m -dependent small GTPase activation. In conclusion, our results reveal a new role for $Na_v1.5$ channels as voltage-dependent activators of Rac1 signaling to promote cellular migration.

ACKNOWLEDGMENTS

This study was supported by the Medical Research Council (G1000508), Cancer Research UK (A25922), and a Radhika V Sreedhar Scholarship.

DATA AVAILABILITY STATEMENT

The data that support the findings of this study are available from the corresponding author upon reasonable request.

CONFLICT OF INTERESTS

The authors declare that there are no conflict of interests.

AUTHOR CONTRIBUTIONS

M. Y. and W. B. contributed to the conception and design of the work. M. Y., A. J., R. K., R. S., P. O., T., and W. B. contributed to acquisition,

analysis, and interpretation of data for the work. M. Y., R. K., R. S., P. O., T., and W. B. contributed to drafting the work and revising it critically for important intellectual content. All authors approved the final version of the manuscript.

ORCID

William J. Brackenbury  <http://orcid.org/0000-0001-6882-3351>

REFERENCES

- Amara, S., Ivy, M. T., Myles, E. L., & Tiriveedhi, V. (2016). Sodium channel γ ENaC mediates IL-17 synergized high salt induced inflammatory stress in breast cancer cells. *Cellular Immunology*, 302, 1–10. <https://doi.org/10.1016/j.cellimm.2015.12.007>
- Antonov, A. S., Antonova, G. N., Fujii, M., ten Dijke, P., Handa, V., Catravas, J. D., & Verin, A. D. (2012). Regulation of endothelial barrier function by TGF- β type I receptor ALK5: Potential role of contractile mechanisms and heat shock protein 90. *Journal of Cellular Physiology*, 227(2), 759–771. <https://doi.org/10.1002/jcp.22785>
- Armstrong, C. M., & Bezanilla, F. (1977). Inactivation of the sodium channel. II. Gating current experiments. *The Journal of General Physiology*, 70(5), 567–590.
- Baldassa, S., Zippel, R., & Sturani, E. (2003). Depolarization-induced signaling to Ras, Rap1 and MAPKs in cortical neurons. *Brain Research: Molecular Brain Research*, 119(1), 111–122.
- Baylor, D. A., & Fettiplace, R. (1977). Transmission from photoreceptors to ganglion cells in turtle retina. *Journal of Physiology*, 271(2), 391–424.
- Beane, W. S., Morokuma, J., Adams, D. S., & Levin, M. (2011). A chemical genetics approach reveals H,K-ATPase-mediated membrane voltage is required for planarian head regeneration. *Chemistry & Biology*, 18(1), 77–89. <https://doi.org/10.1016/j.chembiol.2010.11.012>
- Beane, W. S., Morokuma, J., Lemire, J. M., & Levin, M. (2013). Bioelectric signaling regulates head and organ size during planarian regeneration. *Development*, 140(2), 313–322. <https://doi.org/10.1242/dev.086900>
- Besson, P., Driffort, V., Bon, É., Gradek, F., Chevalier, S., & Roger, S. (2015). How do voltage-gated sodium channels enhance migration and invasiveness in cancer cells? *Biochimica et Biophysica Acta (BBA) - Biomembranes*, 1848(10 Pt B), 2493–2501. <https://doi.org/10.1016/j.bbmem.2015.04.013>
- Beyder, A., Rae, J. L., Bernard, C., Stregge, P. R., Sachs, F., & Farrugia, G. (2010). Mechanosensitivity of Nav1.5, a voltage-sensitive sodium channel. *Journal of Physiology*, 588(Pt 24), 4969–4985. <https://doi.org/10.1113/jphysiol.2010.199034>
- Black, J. A., Dib-Hajj, S., Cohen, S., Hinson, A. W., & Waxman, S. G. (1998). Glial cells have heart: RH1 Na⁺ channel mRNA and protein in spinal cord astrocytes. *Glia*, 23(3), 200–208.
- Black, J. A., Liu, S., & Waxman, S. G. (2009). Sodium channel activity modulates multiple functions in microglia. *Glia*, 57(10), 1072–1081. <https://doi.org/10.1002/glia.20830>
- Black, J. A., & Waxman, S. G. (2013). Noncanonical roles of voltage-gated sodium channels. *Neuron*, 80(2), 280–291. <https://doi.org/10.1016/j.neuron.2013.09.012>
- Blackiston, D. J., McLaughlin, K. A., & Levin, M. (2009). Bioelectric controls of cell proliferation: Ion channels, membrane voltage and the cell cycle. *Cell Cycle*, 8(21), 3527–3536.
- Bourguignon, L. Y. W., Zhu, H., Shao, L., & Chen, Y. W. (2001). CD44 interaction with c-Src kinase promotes cortactin-mediated cytoskeleton function and hyaluronic acid-dependent ovarian tumor cell migration. *Journal of Biological Chemistry*, 276(10), 7327–7336. <https://doi.org/10.1074/jbc.M006498200>
- Brackenbury, W. J. (2012). Voltage-gated sodium channels and metastatic disease. *Channels*, 6(5), 352–361. <https://doi.org/10.4161/chan.21910>
- Brackenbury, W. J. (2016). Ion channels in cancer. In G. S. Pitt (Ed.), *Ion Channels in Health and Disease* (pp. 131–163). Elsevier Inc.
- Brackenbury, W. J., Calhoun, J. D., Chen, C., Miyazaki, H., Nukina, N., Oyama, F., & Ranscht, B. (2010). Functional reciprocity between Na⁺ channel Nav1.6 and 1 subunits in the coordinated regulation of excitability and neurite outgrowth. *Proceedings of the National Academy of Sciences*, 107(5), 2283–2288. <https://doi.org/10.1073/pnas.0909434107>
- Brackenbury, W. J., Chioni, A. M., Diss, J. K. J., & Djamgoz, M. B. A. (2007). The neonatal splice variant of Nav1.5 potentiates in vitro invasive behaviour of MDA-MB-231 human breast cancer cells. *Breast Cancer Research and Treatment*, 101(2), 149–160. <https://doi.org/10.1007/s10549-006-9281-1>
- Brackenbury, W. J., & Djamgoz, M. B. A. (2006). Activity-dependent regulation of voltage-gated Na⁺ channel expression in Mat-LyLu rat prostate cancer cell line: Na⁺ channel autoregulation in Mat-LyLu prostate cancer cells. *Journal of Physiology*, 573(Pt 2), 343–356. <https://doi.org/10.1113/jphysiol.2006.106906>
- Brackenbury, W. J., & Isom, L. L. (2011). Na⁺ channel? Subunits: Overachievers of the ion channel family. *Frontiers in Pharmacology*, 2, 53. <https://doi.org/10.3389/fphar.2011.00053>
- Brackenbury, W. J., Yuan, Y., O'Malley, H. A., Parent, J. M., & Isom, L. L. (2013). Abnormal neuronal patterning occurs during early postnatal brain development of Scn1b-null mice and precedes hyperexcitability. *Proceedings of the National Academy of Sciences*, 110(3), 1089–1094. <https://doi.org/10.1073/pnas.1208767110>
- Bravo-Cordero, J. J., Hodgson, L., & Condeelis, J. (2012). Directed cell invasion and migration during metastasis. *Current Opinion in Cell Biology*, 24(2), 277–283. <https://doi.org/10.1016/j.cceb.2011.12.004>
- Brisson, L., Driffort, V., Benoist, L., Poet, M., Counillon, L., Antelmi, E., & Roger, S. (2013). Nav1.5 Na⁺ channels allosterically regulate the NHE-1 exchanger and promote the activity of breast cancer cell invadopodia. *Journal of Cell Science*, 126(Pt 21), 4835–4842. <https://doi.org/10.1242/jcs.123901>
- Brisson, L., Gillet, L., Calaghan, S., Besson, P., Le Guennec, J. Y., Roger, S., & Gore, J. (2011). Na(V)1.5 enhances breast cancer cell invasiveness by increasing NHE1-dependent H⁺ efflux in caveolae. *Oncogene*, 30(17), 2070–2076. <https://doi.org/10.1038/nc.2010.574>
- Burridge, K., & Wennerberg, K. (2004). Rho and Rac take center stage. *Cell*, 116(2), 167–179.
- Campbell, T. M., Main, M. J., & Fitzgerald, E. M. (2013). Functional expression of the voltage-gated Na⁺-channel Nav1.7 is necessary for EGF-mediated invasion in human non-small cell lung cancer cells. *Journal of Cell Science*, 126(Pt 21), 4939–4949. <https://doi.org/10.1242/jcs.130013>
- Carrithers, M. D., Chatterjee, G., Carrithers, L. M., Offoha, R., Iheagwara, U., Rahner, C., & Waxman, S. G. (2009). Regulation of podosome formation in macrophages by a novel splice variant of the sodium channel SCN8A. *Journal of Biological Chemistry*, 284(12), 8114–8126. <https://doi.org/10.1074/jbc.M801892200>
- Carrithers, M. D., Dib-Hajj, S., Carrithers, L. M., Tokmouline, G., Pypaert, M., Jonas, E. A., & Waxman, S. G. (2007). Expression of the voltage-gated sodium channel Nav1.5 in the macrophage late endosome regulates endosomal acidification. *Journal of Immunology*, 178(12), 7822–7832. <https://doi.org/10.1093/immdev/178.12.7822> [pii].
- Catterall, W. A., Goldin, A. L., & Waxman, S. G. (2003). International Union of Pharmacology. XXXIX. Compendium of voltage-gated ion channels: Sodium channels. *Pharmacological Reviews*, 55(4), 575–578. <https://doi.org/10.1124/pr.55.4.7>
- Cervera, J., Alcaraz, A., & Mafe, S. (2016). Bioelectrical signals and ion channels in the modeling of multicellular patterns and cancer. *Biophysics. Scientific Reports*, 6, 20403. <https://doi.org/10.1038/srep20403>

- Chen, B., Zhang, C., Wang, Z., Chen, Y., Xie, H., Li, S., & Chen, P. (2019). Mechanistic insights into Nav1.7-dependent regulation of rat prostate cancer cell invasiveness revealed by toxin probes and proteomic analysis. *FEBS Journal*, 286(13), 2549–2561. <https://doi.org/10.1111/febs.14823>
- Chernet, B. T., Adams, D. S., Lobikin, M., & Levin, M. (2016). Use of genetically encoded, light-gated ion translocators to control tumorigenesis. *Oncotarget*, <https://doi.org/10.18632/oncotarget.8036>
- Chernet, B. T., & Levin, M. (2014). Transmembrane voltage potential of somatic cells controls oncogene-mediated tumorigenesis at long-range. *Oncotarget*, 5(10), 3287–3306.
- Chifflet, S., Correa, V., Nin, V., Justet, C., & Hernandez, J. A. (2004). Effect of membrane potential depolarization on the organization of the actin cytoskeleton of eye epithelia. The role of adherens junctions. *Experimental Eye Research*, 79(6), 769–777. <https://doi.org/10.1016/j.exer.2004.08.031>
- Chifflet, S., Hernandez, J. A., & Grasso, S. (2005). A possible role for membrane depolarization in epithelial wound healing. *American Journal of Physiology: Cell Physiology*, 288(6), C1420–C1430. <https://doi.org/10.1152/ajpcell.00259.2004>
- Chifflet, S., Hernandez, J. A., Grasso, S., & Cirillo, A. (2003). Nonspecific depolarization of the plasma membrane potential induces cytoskeletal modifications of bovine corneal endothelial cells in culture. *Experimental Cell Research*, 282(1), 1–13.
- Cone, C. D., Jr. (1971). Maintenance of mitotic homeostasis in somatic cell populations. *Journal of Theoretical Biology*, 30(1), 183–194.
- Cone, C. D., Jr., & Cone, C. M. (1976). Induction of mitosis in mature neurons in central nervous system by sustained depolarization. *Science*, 192(4235), 155–158.
- Contreras, G. F., Castillo, K., Enrique, N., Carrasquel-Ursulaez, W., Castillo, J. P., Milesi, V., & Latorre, R. (2013). A BK (Sl α) channel journey from molecule to physiology. *Channels (Austin)*, 7(6), 442–458. <https://doi.org/10.4161/chan.26242>
- Dang, I., Gorelik, R., Sousa-Blin, C., Derivery, E., Guerin, C., Linkner, J., & Gautreau, A. (2013). Inhibitory signalling to the Arp2/3 complex steers cell migration. *Nature*, 503(7475), 281–284. <https://doi.org/10.1038/nature12611>
- Das, S., Yin, T., Yang, Q., Zhang, J., Wu, Y. I., & Yu, J. (2015). Single-molecule tracking of small GTPase Rac1 uncovers spatial regulation of membrane translocation and mechanism for polarized signaling. *Proceedings of the National Academy of Sciences of the United States of America*, 112(3), E267–E276. <https://doi.org/10.1073/pnas.1409667112>
- Djamgoz, M. B., & Onkal, R. (2013). Persistent current blockers of voltage-gated sodium channels: A clinical opportunity for controlling metastatic disease. *Recent Patents on Anti-cancer Drug Discovery*, 8(1), 66–84.
- Driffort, V., Gillet, L., Bon, E., Marionneau-Lambot, S., Oullier, T., Joulin, V., & Roger, S. (2014). Ranolazine inhibits Nav1.5-mediated breast cancer cell invasiveness and lung colonization. *Molecular Cancer*, 13, 264. <https://doi.org/10.1186/1476-4598-13-264>
- Ehrlich, J. S., Hansen, M. D., & Nelson, W. J. (2002). Spatio-temporal regulation of Rac1 localization and lamellipodia dynamics during epithelial cell-cell adhesion. *Developmental Cell*, 3(2), 259–270.
- Fairn, G. D., Schieber, N. L., Ariotti, N., Murphy, S., Kuerschner, L., Webb, R. I., & Parton, R. G. (2011). High-resolution mapping reveals topologically distinct cellular pools of phosphatidylserine. *Journal of Cell Biology*, 194(2), 257–275. <https://doi.org/10.1083/jcb.201012028>. 10.1083/jcb.201012028.
- Finkelstein, C. V., Overduin, M., & Capelluto, D. G. (2006). Cell migration and signaling specificity is determined by the phosphatidylserine recognition motif of Rac1. *Journal of Biological Chemistry*, 281(37), 27317–27326. <https://doi.org/10.1074/jbc.M605560200>
- Fraser, S. P., Ding, Y., Liu, A., Foster, C. S., & Djamgoz, M. B. (1999). Tetrodotoxin suppresses morphological enhancement of the metastatic MAT-LyLu rat prostate cancer cell line. *Cell and Tissue Research*, 295(3), 505–512.
- Fraser, S. P., Diss, J. K., Chioni, A. M., Mycielska, M. E., Pan, H., Yamaci, R. F., & Djamgoz, M. B. (2005). Voltage-gated sodium channel expression and potentiation of human breast cancer metastasis. *Clinical Cancer Research*, 11(15), 5381–5389. <https://doi.org/10.1158/1078-0432.CCR-05-0327>
- Fraser, S. P., Ozerlat-Gunduz, I., Brackenbury, W. J., Fitzgerald, E. M., Campbell, T. M., Coombes, R. C., & Djamgoz, M. B. (2014). Regulation of voltage-gated sodium channel expression in cancer: Hormones, growth factors and auto-regulation. *Philosophical Transactions of the Royal Society of London. Series B: Biological Sciences*, 369(1638), 20130105. <https://doi.org/10.1098/rstb.2013.0105>
- Friedl, P., Locker, J., Sahai, E., & Segall, J. E. (2012). Classifying collective cancer cell invasion. *Nature Cell Biology*, 14(8), 777–783. <https://doi.org/10.1038/ncb2548>
- Fritz, R. D., Menshykau, D., Martin, K., Reimann, A., Pontelli, V., & Pertz, O. (2015). SrGAP2-dependent integration of membrane geometry and slit-robo-repulsive cues regulates fibroblast contact inhibition of locomotion. *Developmental Cell*, 35(1), 78–92. <https://doi.org/10.1016/j.devcel.2015.09.002>
- Garcia-Mata, R., Boulter, E., & BurrIDGE, K. (2011). The 'invisible hand': Regulation of RHO GTPases by RHOGDIs. *Nature Reviews: Molecular Cell Biology*, 12(8), 493–504. <https://doi.org/10.1038/nrm3153>. 10.1038/nrm3153.
- George, A. L., Jr. (2005). Inherited disorders of voltage-gated sodium channels. *Journal of Clinical Investigation*, 115(8), 1990–1999.
- Gillet, L., Roger, S., Besson, P., Lecaille, F., Gore, J., Bougnoux, P., & Le Guennec, J. Y. (2009). Voltage-gated sodium channel activity promotes cysteine cathepsin-dependent invasiveness and colony growth of human cancer cells. *Journal of Biological Chemistry*, 284(13), 8680–8691. <https://doi.org/10.1074/jbc.M806891200>. [pii] 10.1074/jbc.M806891200.
- Grimes, J. A., Fraser, S. P., Stephens, G. J., Downing, J. E., Laniado, M. E., Foster, C. S., & Djamgoz, M. B. (1995). Differential expression of voltage-activated Na⁺ currents in two prostatic tumour cell lines: Contribution to invasiveness in vitro. *FEBS Letters*, 369(2-3), 290–294.
- Heo, W. D., Inoue, T., Park, W. S., Kim, M. L., Park, B. O., Wandless, T. J., & Meyer, T. (2006). PI(3,4,5)P3 and PI(4,5)P2 lipids target proteins with polybasic clusters to the plasma membrane. *Science*, 314(5804), 1458–1461. <https://doi.org/10.1126/science.1134389>
- Hille, B. (1992). *Ionic channels of excitable membranes* (2nd ed.). Sunderland (Massachusetts): Sinauer Associates Inc.
- House, C. D., Vaske, C. J., Schwartz, A., Obias, V., Frank, B., Luu, T., & Lee, N. H. (2010). Voltage-gated Na⁺ channel SCN5A is a key regulator of a gene transcriptional network that controls colon cancer invasion. *Cancer Research*, 70(17), 6957–6967. <https://doi.org/10.1158/0008-5472.CAN-10-1169>
- House, C. D., Wang, B. D., Ceniccola, K., Williams, R., Simaan, M., Olender, J., & Lee, N. H. (2015). Voltage-gated Na⁺ channel activity increases colon cancer transcriptional activity and invasion via persistent MAPK signaling. *Scientific Reports*, 5, 11541. <https://doi.org/10.1038/srep11541>
- Kay, J. G., Koivusalo, M., Ma, X., Wohland, T., & Grinstein, S. (2012). Phosphatidylserine dynamics in cellular membranes. *Molecular Biology of the Cell*, 23(11), 2198–2212. <https://doi.org/10.1091/mbc.E11-11-0936>
- Khaitan, D., Sankpal, U. T., Weksler, B., Meister, E. A., Romero, I. A., Couraud, P. O., & Ningaraj, N. S. (2009). Role of KCNMA1 gene in breast cancer invasion and metastasis to brain. *BMC Cancer*, 9, 258. <https://doi.org/10.1186/1471-2407-9-258>
- Kraft, R., Krause, P., Jung, S., Basrai, D., Liebmann, L., Bolz, J., & Patt, S. (2003). BK channel openers inhibit migration of human glioma cells. *Pflügers Archiv. European Journal of Physiology*, 446(2), 248–255. <https://doi.org/10.1007/s00424-003-1012-4>
- Krause, M., & Gautreau, A. (2014). Steering cell migration: Lamellipodium dynamics and the regulation of directional persistence. *Nature Reviews: Molecular Cell Biology*, 15(9), 577–590. <https://doi.org/10.1038/nrm3861>

- Lee, J. L., Wang, M. J., Sudhir, P. R., & Chen, J. Y. (2008). CD44 engagement promotes matrix-derived survival through the CD44-SRC-integrin axis in lipid rafts. *Molecular and Cellular Biology*, 28(18), 5710–5723. <https://doi.org/10.1128/MCB.00186-08>
- Li, Q., Lau, A., Morris, T. J., Guo, L., Fordyce, C. B., & Stanley, E. F. (2004). A syntaxin 1, Galpha(o), and N-type calcium channel complex at a presynaptic nerve terminal: Analysis by quantitative immunocolocalization. *Journal of Neuroscience*, 24(16), 4070–4081. <https://doi.org/10.1523/JNEUROSCI.0346-04.2004>
- Lobikin, M., Chernet, B., Lobo, D., & Levin, M. (2012). Resting potential, oncogene-induced tumorigenesis, and metastasis: The bioelectric basis of cancer in vivo. *Physical Biology*, 9(6), 065002. <https://doi.org/10.1088/1478-3975/9/6/065002>
- Lobikin, M., Lobo, D., Blackiston, D. J., Martyniuk, C. J., Tkachenko, E., & Levin, M. (2015). Serotonergic regulation of melanocyte conversion: A bioelectrically regulated network for stochastic all-or-none hyperpigmentation. *Science Signaling*, 8(397), ra99. <https://doi.org/10.1126/scisignal.aac6609>
- Ma, Y. G., Liu, W. C., Dong, S., Du, C., Wang, X. J., Li, J. S., & Xie, M. J. (2012). Activation of BK(Ca) channels in zoledronic acid-induced apoptosis of MDA-MB-231 breast cancer cells. *PLOS One*, 7(5), e37451. <https://doi.org/10.1371/journal.pone.0037451>
- Machacek, M., Hodgson, L., Welch, C., Elliott, H., Pertz, O., Nalbant, P., & Danuser, G. (2009). Coordination of Rho GTPase activities during cell protrusion. *Nature*, 461(7260), 99–103. <https://doi.org/10.1038/nature08242>
- Macmillan, S., Sheridan, R. D., Chilvers, E. R., & Patmore, L. (1995). A comparison of the effects of SCA40, NS 004 and NS 1619 on large conductance Ca(2+)-activated K+ channels in bovine tracheal smooth muscle cells in culture. *British Journal of Pharmacology*, 116(1), 1656–1660. Retrieved from <http://dx.doi.org/>
- Magalhaes, M. A. O., & Glogauer, M. (2010). Pivotal advance: Phospholipids determine net membrane surface charge resulting in differential localization of active Rac1 and Rac2. *Journal of Leukocyte Biology*, 87(4), 545–555. <https://doi.org/10.1189/jlb.0609390>
- Manders, E. M. M., Verbeek, F. J., & Aten, J. A. (1993). Measurement of colocalization of objects in dual-colour confocal images. *Journal of Microscopy*, 169(3), 375–382. <https://doi.org/10.1111/j.1365-2818.1993.tb03313.x>
- Marei, H., & Malliri, A. (2017). GEFs: Dual regulation of Rac1 signaling. *Small GTPases*, 8(2), 90–99. <https://doi.org/10.1080/21541248.2016.1202635>
- Marrison, J., Raty, L., Marriott, P., & O'Toole, P. (2013). Ptychography--a label free, high-contrast imaging technique for live cells using quantitative phase information. *Scientific Reports*, 3, 2369. <https://doi.org/10.1038/srep02369>
- Martin, F., Ufodiama, C., Watt, I., Bland, M., & Brackenbury, W. J. (2015). Therapeutic value of voltage-gated sodium channel inhibitors in breast, colorectal and prostate cancer: A systematic review. *Frontiers in Pharmacology*, 6, 273. <https://doi.org/10.3389/fphar.2015.00273>
- Masters, J. R., Thomson, J. A., Daly-Burns, B., Reid, Y. A., Dirks, W. G., Packer, P., & Debenham, P. G. (2001). Short tandem repeat profiling provides an international reference standard for human cell lines. *Proceedings of the National Academy of Sciences of the United States of America*, 98(14), 8012–8017. <https://doi.org/10.1073/pnas.121616198>
- Moissoglu, K., Slepchenko, B. M., Meller, N., Horwitz, A. F., & Schwartz, M. A. (2006). In vivo dynamics of Rac-membrane interactions. *Molecular Biology of the Cell*, 17(6), 2770–2779. <https://doi.org/10.1091/mbc.E06-01-0005>
- Nelson, M., Millican-Slater, R., Forrest, L. C., & Brackenbury, W. J. (2014). The sodium channel beta1 subunit mediates outgrowth of neurite-like processes on breast cancer cells and promotes tumour growth and metastasis. *International Journal of Cancer*, 135(10), 2338–2351. <https://doi.org/10.1002/ijc.28890>
- Nelson, M., Yang, M., Dowle, A. A., Thomas, J. R., & Brackenbury, W. J. (2015). The sodium channel-blocking antiepileptic drug phenytoin inhibits breast tumour growth and metastasis. *Molecular Cancer*, 14(1), 13. <https://doi.org/10.1186/s12943-014-0277-x>
- Nelson, M., Yang, M., Millican-Slater, R., & Brackenbury, W. J. (2015). Nav1.5 regulates breast tumor growth and metastatic dissemination in vivo. *Oncotarget*, 6(32), 32914–32929. <https://doi.org/10.18632/oncotarget.5441>
- Nin, V., Hernandez, J. A., & Chifflet, S. (2009). Hyperpolarization of the plasma membrane potential provokes reorganization of the actin cytoskeleton and increases the stability of adherens junctions in bovine corneal endothelial cells in culture. *Cell Motility and the Cytoskeleton*, 66(12), 1087–1099. <https://doi.org/10.1002/cm.20416>
- Pappalardo, L. W., Samad, O. A., Black, J. A., & Waxman, S. G. (2014). Voltage-gated sodium channel Nav 1.5 contributes to astroglial injury in an in vitro model of glial injury via reverse Na+ /Ca2+ exchange. *Glia*, 62(7), 1162–1175. <https://doi.org/10.1002/glia.22671>
- Patel, F., & Brackenbury, W. J. (2015). Dual roles of voltage-gated sodium channels in development and cancer. *International Journal of Developmental Biology*, 59, 357–366. <https://doi.org/10.1387/ijdb.150171wb>
- Persson, A. K., Estacion, M., Ahn, H., Liu, S., Stamboulian-Platel, S., Waxman, S. G., & Black, J. A. (2014). Contribution of sodium channels to lamellipodial protrusion and Rac1 and ERK1/2 activation in ATP-stimulated microglia. *Glia*, 62(12), 2080–2095. <https://doi.org/10.1002/glia.22728>
- Pollard, T. D. (2007). Regulation of actin filament assembly by Arp2/3 complex and formins. *Annual Review of Biophysics and Biomolecular Structure*, 36, 451–477. <https://doi.org/10.1146/annurev.biophys.35.040405.101936>
- Prevarskaya, N., Skryma, R., & Shuba, Y. (2018). Ion channels in cancer: Are cancer hallmarks oncochannelopathies? *Physiological Reviews*, 98(2), 559–621. <https://doi.org/10.1152/physrev.00044.2016>
- Remorino, A., De Beco, S., Cayrac, F., Di Federico, F., Cornilleau, G., Gautreau, A., & Coppey, M. (2017). Gradients of Rac1 nanoclusters support spatial patterns of Rac1 signaling. *Cell Reports*, 21(7), 1922–1935. <https://doi.org/10.1016/j.celrep.2017.10.069>
- Ridley, A. J. (2011). Life at the leading edge. *Cell*, 145(7), 1012–1022. <https://doi.org/10.1016/j.cell.2011.06.010>
- Ridley, A. J. (2015). Rho GTPase signalling in cell migration. *Current Opinion in Cell Biology*, 36, 103–112. <https://doi.org/10.1016/j.ceb.2015.08.005>
- Roger, S., Besson, P., & Le Guennec, J. Y. (2003). Involvement of a novel fast inward sodium current in the invasion capacity of a breast cancer cell line. *Biochimica et Biophysica Acta*, 1616(2), 107–111.
- Roger, S., Potier, M., Vandier, C., Le Guennec, J. Y., & Besson, P. (2004). Description and role in proliferation of ibertoxin-sensitive currents in different human mammary epithelial normal and cancerous cells. *Biochimica et Biophysica Acta*, 1667(2), 190–199. <https://doi.org/10.1016/j.bbamem.2004.10.002>
- Roger, S., Rollin, J., Barascu, A., Besson, P., Raynal, P. I., Lochmann, S., & Le Guennec, J. Y. (2007). Voltage-gated sodium channels potentiate the invasive capacities of human non-small-cell lung cancer cell lines. *International Journal of Biochemistry and Cell Biology*, 39(4), 774–786. <https://doi.org/10.1016/j.biocel.2006.12.007>
- Sanguinetti, M. C., & Jurkiewicz, N. K. (1990). Two components of cardiac delayed rectifier K+ current. Differential sensitivity to block by class III antiarrhythmic agents. *Journal of General Physiology*, 96(1), 195–215.
- Sareen, D., Darjatmoko, S. R., Albert, D. M., & Polans, A. S. (2007). Mitochondria, calcium, and calpain are key mediators of resveratrol-induced apoptosis in breast cancer. *Molecular Pharmacology*, 72(6), 1466–1475. <https://doi.org/10.1124/mol.107.039040>
- Schneider, C. A., Rasband, W. S., & Eliceiri, K. W. (2012). NIH Image to ImageJ: 25 years of image analysis. *Nature Methods*, 9(7), 671–675.
- Schwab, A., Fabian, A., Hanley, P. J., & Stock, C. (2012). Role of ion channels and transporters in cell migration. *Physiological Reviews*, 92(4), 1865–1913. <https://doi.org/10.1152/physrev.00018.2011>
- Servitja, J. M., Marinissen, M. J., Sodhi, A., Bustelo, X. R., & Gutkind, J. S. (2003). Rac1 function is required for Src-induced transformation.

- Evidence of a role for Tiam1 and Vav2 in Rac activation by Src. *Journal of Biological Chemistry*, 278(36), 34339–34346. <https://doi.org/10.1074/jbc.M302960200>
- Sontheimer, H., Fernandez-Marques, E., Ullrich, N., Pappas, C. A., & Waxman, S. G. (1994). Astrocyte Na⁺ channels are required for maintenance of Na⁺/K⁺-ATPase activity. *Journal of Neuroscience*, 14(5 Pt 1), 2464–2475. <http://www.jneurosci.org/content/jneuro/14/5/2464.full.pdf>.
- Stock, C., & Schwab, A. (2015). Ion channels and transporters in metastasis. *Biochimica et Biophysica Acta/Biomembranes*, 1848(10 Pt B), 2638–2646. <https://doi.org/10.1016/j.bbmem.2014.11.012>
- Stys, P. K., Sontheimer, H., Ransom, B. R., & Waxman, S. G. (1993). Noninactivating, tetrodotoxin-sensitive Na⁺ conductance in rat optic nerve axons. *Proceedings of the National Academy of Sciences of the United States of America*, 90(15), 6976–6980. <https://www.pnas.org/content/pnas/90/15/6976.full.pdf>.
- Suman, R., Smith, G., Hazel, K. E., Kasprovicz, R., Coles, M., O'Toole, P., & Chawla, S. (2016). Label-free imaging to study phenotypic behavioural traits of cells in complex co-cultures. *Scientific Reports*, 6, 22032. <https://doi.org/10.1038/srep22032>
- Sundelacruz, S., Levin, M., & Kaplan, D. L. (2008). Membrane potential controls adipogenic and osteogenic differentiation of mesenchymal stem cells. *PLOS One*, 3(11), e3737. <https://doi.org/10.1371/journal.pone.0003737>
- Sundelacruz, S., Levin, M., & Kaplan, D. L. (2009). Role of membrane potential in the regulation of cell proliferation and differentiation. *Stem Cell Reviews*, 5(3), 231–246. <https://doi.org/10.1007/s12015-009-9080-2>
- Szaszi, K., Sirokmany, G., Di Ciano-Oliveira, C., Rotstein, O. D., & Kapus, A. (2005). Depolarization induces Rho-Rho kinase-mediated myosin light chain phosphorylation in kidney tubular cells. *American Journal of Physiology: Cell Physiology*, 289(3), C673–C685. <https://doi.org/10.1152/ajpcell.00481.2004>
- Ulbricht, W. (1998). Effects of veratridine on sodium currents and fluxes. *Reviews of Physiology Biochemistry and Pharmacology*, 133, 1–54.
- Uphoff, C. C., Gignac, S. M., & Drexler, H. G. (1992). Mycoplasma contamination in human leukemia cell lines. I. Comparison of various detection methods. *Journal of Immunological Methods*, 149(1), 43–53.
- van Hennik, P. B., ten Klooster, J. P., Halstead, J. R., Voermans, C., Anthony, E. C., Divecha, N., & Hordijk, P. L. (2003). The C-terminal domain of Rac1 contains two motifs that control targeting and signaling specificity. *Journal of Biological Chemistry*, 278(40), 39166–39175. <https://doi.org/10.1074/jbc.M307001200>
- Waheed, F., Speight, P., Kawai, G., Dan, Q., Kapus, A., & Szaszi, K. (2010). Extracellular signal-regulated kinase and GEF-H1 mediate depolarization-induced Rho activation and paracellular permeability increase. *American Journal of Physiology: Cell Physiology*, 298(6), C1376–C1387. <https://doi.org/10.1152/ajpcell.00408.2009>
- Winnicka, K., Bielawski, K., Bielawska, A., & Surazynski, A. (2008). Antiproliferative activity of derivatives of ouabain, digoxin and proscillaridin A in human MCF-7 and MDA-MB-231 breast cancer cells. *Biological & Pharmaceutical Bulletin*, 31(6), 1131–1140.
- Wu, Y. I., Frey, D., Lungu, O. I., Jaehrig, A., Schlichting, I., Kuhlman, B., & Hahn, K. M. (2009). A genetically encoded photoactivatable Rac controls the motility of living cells. *Nature*, 461(7260), 104–108. <https://doi.org/10.1038/nature08241>
- Yang, M., & Brackenbury, W. J. (2013). Membrane potential and cancer progression. *Frontiers in Physiology*, 4, 185. <https://doi.org/10.3389/fphys.2013.00185>
- Yang, M., Kozminski, D. J., Wold, L. A., Modak, R., Calhoun, J. D., Isom, L. L., & Brackenbury, W. J. (2012). Therapeutic potential for phenytoin: Targeting Na(v)1.5 sodium channels to reduce migration and invasion in metastatic breast cancer. *Breast Cancer Research and Treatment*, 134(2), 603–615. <https://doi.org/10.1007/s10549-012-2102-9>
- Yildirim, S., Altun, S., Gumushan, H., Patel, A., & Djamgoz, M. B. (2012). Voltage-gated sodium channel activity promotes prostate cancer metastasis in vivo. *Cancer Letters*, 323(1), 58–61. <https://doi.org/10.1016/j.canlet.2012.03.036>
- Zhou, Y., Wong, C. O., Cho, K. J., van der Hoeven, D., Liang, H., Thakur, D. P., & Hancock, J. F. (2015). Membrane potential modulates plasma membrane phospholipid dynamics and K-Ras signaling. *Science*, 349(6250), 873–876. <https://doi.org/10.1126/science.aaa5619>

SUPPORTING INFORMATION

Additional supporting information may be found online in the Supporting Information section.

How to cite this article: Yang M, James AD, Suman R, et al. Voltage-dependent activation of Rac1 by Na_v1.5 channels promotes cell migration. *J Cell Physiol*. 2020;235:3950–3972. <https://doi.org/10.1002/jcp.29290>